

CONVECTIVE HEAT AND MASS TRANSFER FLOW OF A MICROPOLAR FLUID
IN A RECTANGULAR DUCT WITH NON LINEAR DENSITY TEMPERATURE

Dr. R. SIVA GOPAL*¹, Prof. R. SIVA PRASAD²

^{1,2}Department of Mathematics,
S. K. University, Anantapuramu-515003, (A.P.), India.

(Received On: 15-12-17; Revised & Accepted On: 21-01-18)

ABSTRACT

We make an investigation of the convective heat and mass transfer flow of a micropolar fluid in a rectangular duct with non linear density temperature. The equations governing the flow of heat and mass transfer are non linear coupled equations. It is not possible to find closed form solutions; therefore we solve these equations by using Galerkin finite element analysis with three noded triangular elements. The temperature, concentration and angular velocity distributions are analyzed for different values of G , R , D^{-1} , P , Sc , γ , α , λ and N . The rate of heat and mass transfer and couple stress evaluated numerically for a different parametric values.

Keywords: Heat and Mass Transfer, Rectangular Duct, Temperature, Micropolar fluid, Density.

1. INTRODUCTION

Natural convection is of great importance in many applications of industries. Convection plays an authoritative role in crystal growth on which it affects the composition of fluid phase and temperature at the phase interface whose consequence results in a single crystal poor crystal quality is due to turbulence. It is the base in modern electronics industry to produce pure and perfect crystals that are used to make laser rods, transistors. Infrared detectors, microwave devices, memory devices, and Ic's (Integrated circuits). Natural convection harmfully affects local growth conditions and increases the overall transport rate. As high power electronic packaging and component density keep increasing substantially with the fast growth of electronic technology, effective cooling of electronic equipment has become exceptionally necessary. Therefore, the natural convection in an enclosure has become increasingly important in engineering applications in recent years. Through studies of the thermal behavior of the fluid in a partitioned enclosure is helpful to understand the more complex processes of natural convection in practical applications number of studies, numerical and experimental, concerned with the natural convection in an enclosure with or without a divider were conducted in past years.

Convective heat transfer in a porous duct which is rectangular and the vertical walls are maintained at two different temperatures and the horizontal walls being insulated is a problem which has grabbed interest by several authors verschuur and greebler [26] have investigated heat transfer in enclosures experimentally. From the literature we find that the influence of viscous dissipation on heat transfer has been examined for different shapes. kamotoni *et.al* [15] has examined Experimental study of natural convection in shallow enclosures with horizontal temperature and concentration gradients.

Shanthy *et.al* [23] has examined Finite element analysis of convective heat and mass transfer flow of a viscous electrically conducting fluid through a porous medium in a rectangular cavity with dissipation. She has examined the influence of dissipation on radiation on double diffusive flow of a viscous fluid in the rectangular cavity. Umadevi *et.al* [24] has examined Finite Element Analysis of double-diffusive heat transfer flow in rectangular duct with thermo-diffusion and radiation effects under inclined magnetic field. Chamka *et.al* [5, 6] have examined, Unsteady MHD Convective Heat and Mass transfer past a semi-infinite vertical permeable moving plate with heat absorption, Heat and mass transfer in a porous medium filled rectangular duct with Soret and Dufour effects under inclined magnetic field. Several relevant analytical and experimental studies have been reported during the past decades. Excellent reviews have been given by Ostrach [17] and Catton [3, 4]. Samuels and Churchill [21] presented the stability of fluids in rectangular region heated from below and obtained the critical Rayleigh numbers with finite differences approximation.

Corresponding Author: Dr. R. Siva Gopal*¹,

¹Department of Mathematics, S. K. University, Anantapuramu-515003, (A.P.), India.

Ozoe *et.al* [18, 19] determined experimentally and numerically the natural convection in an inclined long channel with a rectangular cross-section, and found the effects of inclination angle and aspect ratio on the circulation and rate of heat transfer. Sessa sailaja *et.al* [22] studied Effect of non-linear density temperature variation on convective heat transfer of a viscous fluid through a rectangular cavity. Al-Nimr [1] discussed analytical solution for transient laminar fully developed free convection in vertical annulai. The theory of micropolar fluids developed by Erigen [9, 10 and 11] has been a popular filed of research in recent years. In this theory, the local effects arising from the microstructure and the intrinsic motions of the fluid elements are taken into account. It has been expected to describe properly the non-Newtonian behavior of certain fluids, such as liquid crystals, ferro liquids, colloidal fluid, and liquids with polymer additives. Recently, Jena and Bhattacharya [14] studied the effect of microstructure on the thermal convection in a rectangular box heated from below with Galerkin's method, and obtained critical Rayleigh numbers for various material parameters. Badruddin *et.al* [2] has examined Heat transfer in porous cavity under the influence of radiation and viscous dissipation. Gnanaprasunamba *et.al* [12] studied Convective heat and mass transfer flow of a Rectangular Duct With solet and dufour effects and heat sources. Rajakumari [20] have studied Convective Heat and Mass Transfer flow Micro polar fluid in a Rectangular duct with heat sources. Wang *et.al* [28, 29] presented the study of the natural convection of micropolar fluids in an inclined rectangular enclosure. Cha-Kaungchen *et.al* [7] have investigated numerically the steady laminar natural convection flow of a micropolar fluid in a rectangular enclosure.

Wilson and Rydin [30] discussed bifurcation phenomenon in a rectangular cavity. Veera Suneela Rani *et.al* [25] discussed Radiation Effects on Convective Heat and Mass Transfer Flow in a Rectangular Cavity. The effect of the highest on the location of the divider is investigated. Also the effects of material parameters or micropolar fluids. Davis *et.al* [8] have investigated the effects, the characteristic parameters of micropolar fluids on mixed convection in a cavity.

2. FORMULATION OF THE PROBLEM

We consider the mixed convective heat and mass transfer flow of a viscous, incompressible, micropolar fluid in a saturated porous medium confined in the rectangular duct whose base length is a and height b . The heat flux on the base and top walls is maintained constant. The Cartesian coordinate system is chosen with origin on the central axis of the duct and its base parallel to X-axis, we assume that

- (i) The convective fluid and the porous medium are everywhere in local thermo dynamic equilibrium.
- (ii) There is no phase change of the fluid in the medium.
- (iii) The properties of the fluid and of the porous medium are homogeneous and isotropic.
- (iv) The porous medium is assumed to be closely packed so that Darcy's momentum law is adequate in the porous medium.
- (v) The Boussinesq approximation is applicable,

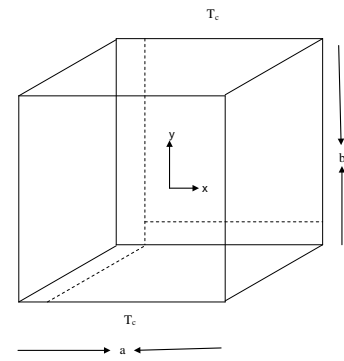


Fig.1
SCHEMATIC DIAGRAM OF THE FLOW MODEL

Under the assumption the governing equations are given by

$$\frac{\partial u'}{\partial x'} + \frac{\partial v'}{\partial y'} = 0 \tag{1}$$

$$-\frac{\partial p}{\partial x'} - \frac{(\mu + k)}{k_1} u + k \frac{\partial \omega}{\partial y'} = 0 \tag{2}$$

$$-\frac{\partial p}{\partial x'} - \frac{(\mu + k)}{k_1} v + k \frac{\partial \omega}{\partial y'} - \rho g' = 0 \tag{3}$$

$$\rho_\sigma C_p \left[u' \frac{\partial T'}{\partial x'} + v' \frac{\partial T'}{\partial y'} \right] = k_f \left[\frac{\partial^2 T'}{\partial x'^2} + \frac{\partial^2 T'}{\partial y'^2} \right] \tag{4}$$

$$\rho_j \left[u' \frac{\partial \omega}{\partial x'} + v' \frac{\partial \omega}{\partial y'} \right] = \gamma \left[\frac{\partial^2 \omega}{\partial x'^2} + \frac{\partial^2 \omega}{\partial y'^2} \right] + K \left(\frac{\partial v'}{\partial x'} - \frac{\partial u'}{\partial y'} - 2\omega \right) \tag{5}$$

$$\rho_\sigma C_p \left[u' \frac{\partial C}{\partial x'} + v' \frac{\partial C}{\partial y'} \right] = D_m \left[\frac{\partial^2 C}{\partial x'^2} + \frac{\partial^2 C}{\partial y'^2} \right] \tag{6}$$

$$\rho' = \rho_0 \{ 1 - \beta_0 (T - T_0) - \beta_1 (T - T_0)^2 - \beta^* (C - C_0) \}$$

$$T_0 = \frac{T_h + T_c}{2},$$

$$C_0 = \frac{C_h + C_c}{2} \quad (7)$$

where u' and v' are Darcy velocities along direction. T' , C , p' and g' are the temperature, micro rotation, pressure and acceleration due to gravity, T_c and T_h are the temperature on the cold and warm side walls respectively. ρ , μ , ν , β_0 and β_1 are the density, coefficients of viscosity, kinematic viscosity and thermal expansion of the fluid, β^* volumetric expansion with mass Fraction k_1 is the permeability of the porous medium, γ_1 , k are the micropolar and material constant pressure.

The boundary conditions are

$$\begin{aligned} u' = v' = 0 & \quad \text{on the boundary of the duct} \\ T' = T_h, C=C_h & \quad \text{on the side wall to the right (x = 1)} \\ T' = T_c, C=C_c & \quad \text{on the side wall to the left (x = 0)} \\ \frac{\partial T'}{\partial y} = 0, \frac{\partial C}{\partial y} = 0 & \quad \text{on the top (y = 0) and bottom} \end{aligned} \quad (8)$$

$u = v = 0$ walls (y = 0) which are insulated,

$$\left. \begin{aligned} \omega &= \frac{-1}{2} \frac{\partial u}{\partial x} \quad \text{On } y = 0 \text{ \& } 1 \\ \omega &= \frac{-1}{2} \frac{\partial v}{\partial x} \quad \text{On } x = 0 \text{ \& } 1 \end{aligned} \right\} \quad (9)$$

Eliminating the pressure p from equations (2) and (3) and using (6) we get

$$0 = \frac{-(\mu + k)}{k_1} \left(\frac{\partial u'}{\partial y'} - \frac{\partial v'}{\partial x'} \right) + k \left(\frac{\partial^2 u'}{\partial y'^2} - \frac{\partial^2 v'}{\partial x'^2} \right) + \rho' \beta g' \left(\frac{\partial}{\partial x'} (T' - T_0) + \rho' \beta^* g' \frac{\partial}{\partial x'} (C - C_0) \right) \quad (10)$$

On introducing the stream function Ψ as

$$u' = -\frac{\partial \Psi}{\partial y'}, \quad v' = \frac{\partial \Psi}{\partial x'}$$

The equations (10) and (5) reduce to

$$\frac{(\mu + k)}{k_1} \nabla^2 \Psi + k \nabla^2 \omega + (\beta_0 g' \frac{\partial}{\partial x'} (T' - T_0) + 2\beta_1 g' (T' - T_0) \frac{\partial}{\partial x'} (T' - T_0) + \beta^* g' \frac{\partial}{\partial x'} (C - C_0)) \quad (11)$$

$$\rho_0 C_p \left(\frac{\partial \Psi}{\partial x'} \frac{\partial T'}{\partial y'} - \frac{\partial \Psi}{\partial y'} \frac{\partial T'}{\partial x'} \right) = k_f \nabla^2 T' - Q(T' - T_0) + \left(\frac{\mu}{k_1} \right) \left(\left(\frac{\partial \Psi}{\partial x'} \right)^2 + \left(\frac{\partial \Psi}{\partial y'} \right)^2 \right) \quad (12)$$

$$\rho_j \left(\frac{\partial \Psi}{\partial x'} \frac{\partial \Psi}{\partial y'} - \frac{\partial \Psi}{\partial y'} \frac{\partial \Psi}{\partial x'} \right) = \gamma_1 \nabla^2 \omega + K(\nabla^2 \Psi - 2\omega) \quad (13)$$

$$\left(\frac{\partial \Psi}{\partial x'} \frac{\partial C}{\partial y'} - \frac{\partial \Psi}{\partial y'} \frac{\partial C}{\partial x'} \right) = D_m \nabla^2 C \quad (14)$$

Now introducing the following non-dimensional variables

$$\begin{aligned} x' &= ax, \quad y' = by \\ h &= \frac{b}{a}, \quad \Psi' = \frac{\Psi}{\nu} \end{aligned}$$

$$u' = \left(\frac{\nu}{a} \right) u \quad v' = \left(\frac{\nu}{a} \right) v \quad p' = \left(\frac{\nu^2 \rho}{a^2} \right) p$$

$$T' = T_c + \theta(T_h - T_c)$$

$$\omega^1 = \begin{pmatrix} \frac{\omega}{v} \\ \frac{v}{a^{22}} \end{pmatrix}$$

$$C' = C_c + C(C_h - C_c) \tag{15}$$

The equations (11) – (13) in the non-dimensional form are

$$\nabla^2 \Psi = -RD^{-1} \nabla^2 \omega - GD^{-1} \left(\frac{\partial \theta}{\partial x} + 2r_1 \theta \frac{\partial \theta}{\partial x} + N \frac{\partial C}{\partial x} \right) \tag{16}$$

$$P \left[\frac{\partial \Psi}{\partial x} \frac{\partial \theta}{\partial y} - \frac{\partial \Psi}{\partial y} \frac{\partial \theta}{\partial x} \right] = \left[\frac{\partial^2 \theta}{\partial x^2} + \frac{\partial^2 \theta}{\partial y^2} \right] \tag{17}$$

$$\nabla^2 \omega + 2 \left(\frac{R}{\lambda} \right) \omega = \left(\frac{R}{\lambda} \right) \nabla^2 \Psi \tag{18}$$

$$Sc \left[\frac{\partial \Psi}{\partial x} \frac{\partial C}{\partial y} - \frac{\partial \Psi}{\partial y} \frac{\partial C}{\partial x} \right] = \left[\frac{\partial^2 C}{\partial x^2} + \frac{\partial^2 C}{\partial y^2} \right] \tag{19}$$

The non dimensional boundary conditions are

$Y = \Psi_x = 0$ on the boundary

$\theta = 1, C=1$ on $x = 1$

$\theta = 0, C=0$ on $x = 0$

$$\left. \begin{aligned} \omega &= \frac{1}{2} \frac{\partial^2 \Psi}{\partial x \partial y} && \text{on } y = 0 \text{ \& } 1 \\ \omega &= -\frac{1}{2} \frac{\partial^2 \Psi}{\partial y \partial x} && \text{on } x = 0 \text{ \& } 1 \end{aligned} \right\}$$

where

$$G = \frac{g\beta(T_h - T_c)a^3}{v^2} \text{ Grashof number, } P = \mu C_p / k_f \text{ Prandtl number}$$

$$D^{-1} = \frac{a^2}{k_1} \text{ Inverse Darcy parameter, } R = \frac{k}{\mu} \text{ Micropolar parameter}$$

$$\lambda = \frac{\gamma}{va^2} \text{ Micropolar material constant, } \gamma = \beta_1 \Delta T / \beta_0 \text{ Density ratio}$$

$$Sc = \frac{v}{D_m} \text{ Schmidt number, } N = \frac{\beta^*(C_h - C_c)}{\beta(T_h - T_c)} \text{ Buoyancy ratio}$$

3. SOLUTION OF THE PROBLEM

Finite Element Analysis

The region is divided into a finite number of three noded triangular elements, in each of which the element equation is derived using Galerkin weighted residual method. In each element f_i the approximate solution for an unknown f in the variation formulation is expressed as a linear combination of shape function (N_k^i) $k = 1, 2, 3$, which are linear polynomials $\sin x$ and y . This approximate solution of the unknown f coincides with actual values of each node of the element. The variation formulation results in 3x3 matrix equation (stiffness matrix) for the unknown local nodal values of the given element. The stiffness matrices are assembled in terms of global nodal values using inter element continuity and boundary conditions resulting in global matrix equation.

In each case there are r distinct global nodes in the finite element domain and $f_p = (p = 1, 2...r)$ is the global nodal values of any unknown f defined over the domain

$$\text{Then } f = \sum_{\alpha=1}^s \sum_{p=1}^r f_p \phi_p' \quad (20)$$

Where the first summation denotes summation over s elements and the second one represents summation over the independent global nodes and $\phi_p^i = N_N^i$, if p is one of the local nodes say k of the element $e_i = 0$, f_p' s are determined from the global matrix equation. Based on these lines we now make a finite element analysis of the given problem governed by (14) – (16) subject to the conditions.

Let ψ^i, θ^i and N^i be the approximate values ψ, θ and N in a element e_i

$$\begin{aligned} \Psi^i &= N_1^i \Psi_1^i + N_2^i \Psi_2^i + N_3^i \Psi_3^i \\ \theta^i &= N_1^i \theta_1^i + N_2^i \theta_2^i + N_3^i \theta_3^i \\ C^i &= N_1^i C_1^i + N_2^i C_2^i + N_3^i C_3^i \\ \omega^i &= N_1^i \omega_1^i + N_2^i \omega_2^i + N_3^i \omega_3^i \end{aligned} \quad (21)$$

Substituting the approximate value ψ^i, θ^i, C^i and ω^i for Ψ, θ, C and ω respectively in (14)

$$E_1^i = \left(\frac{\partial^2 \theta^i}{\partial x^2} \right) + \frac{\partial^2 \theta^i}{\partial y^2} - P \left[\frac{\partial \Psi^i}{\partial y} \frac{\partial \theta^i}{\partial x} - \frac{\partial \Psi^i}{\partial x} \frac{\partial \theta^i}{\partial y} \right] \quad (22)$$

$$E_2^i = \frac{\partial^2 \omega^i}{\partial x^2} + \frac{\partial^2 \omega^i}{\partial y^2} + 2R\omega^i - \frac{R}{\lambda} \left(\frac{\partial^2 \Psi^i}{\partial x^2} + \frac{\partial^2 \Psi^i}{\partial y^2} \right) \quad (23)$$

Under Galaerkin method this is made orthogonal over the domain e_i to the respective shape functions (weight function)

$$\begin{aligned} \text{Where } \int_{e_i} E_1^i N_k^i d\Omega &= 0 \\ \int_{e_i} E_2^i N_k^i d\Omega &= 0 \end{aligned} \quad (24)$$

$$\begin{aligned} \Rightarrow \int_{e_i} N_k^i \left(\frac{\partial^2 \theta^i}{\partial x^2} \right) + \frac{\partial^2 \theta^i}{\partial y^2} + P \left[\frac{\partial \Psi^i}{\partial y} \frac{\partial \theta^i}{\partial x} - \frac{\partial \Psi^i}{\partial x} \frac{\partial \theta^i}{\partial y} \right] d\Omega &= 0 \\ \int_{e_i} N_k^i \left[\frac{\partial^2 \omega^i}{\partial x^2} + \frac{\partial^2 \omega^i}{\partial y^2} \right] + 2R\omega^i - \frac{R}{\lambda} \left(\frac{\partial^2 \Psi^i}{\partial x^2} + \frac{\partial^2 \Psi^i}{\partial y^2} \right) d\Omega &= 0 \end{aligned} \quad (25)$$

Using Green's theorem we reduce the surface integral (24) and (25) without affecting ψ terms and obtain

$$\int_{e_i} N_k^i \left\{ \frac{\partial N_k^i}{\partial x} \frac{\partial \theta^i}{\partial x} + \frac{\partial N_k^i}{\partial y} \frac{\partial \theta^i}{\partial y} - P N_k^i \left[\frac{\partial \Psi^i}{\partial y} \frac{\partial \theta^i}{\partial x} - \frac{\partial \Psi^i}{\partial x} \frac{\partial \theta^i}{\partial y} \right] \right\} d\Omega = \int_{\Gamma_i} N_k^i \left(\frac{\partial \theta^i}{\partial x} nx + \frac{\partial \theta^i}{\partial y} ny \right) d\Gamma_i \quad (26)$$

$$\begin{aligned} \int_{e_i} N_k^i \left\{ \frac{\partial N_k^i}{\partial x} \frac{\partial \omega^i}{\partial x} + \frac{\partial N_k^i}{\partial y} \frac{\partial \omega^i}{\partial y} \right\} + 2R\omega^i - \frac{R}{\lambda} \left(\frac{\partial N_k^i}{\partial x} \frac{\partial \Psi^i}{\partial x} + \frac{\partial N_k^i}{\partial y} \frac{\partial \Psi^i}{\partial y} \right) \\ = \int_{\Gamma_i} N_k^i \left[\left(\frac{\partial \omega^i}{\partial x} - \frac{R}{\lambda} \frac{\partial \Psi^i}{\partial x} \right) nx + \left(\frac{\partial \omega^i}{\partial y} - \frac{R}{\lambda} \frac{\partial \Psi^i}{\partial y} \right) ny + \right] d\Gamma_i \end{aligned} \quad (27)$$

where Γ_1 is the boundary of e_i , substituting for ψ^i, θ^i, C^i and ω^i in equation (26) and eqn (27) we get

$$\begin{aligned} \sum_{i=1}^3 \int_{e_i} \frac{\partial N_k^i}{\partial x} \frac{\partial N_L^i}{\partial x} - \frac{\partial N_L^i}{\partial y} \frac{\partial N_k^i}{\partial y} - P \sum_{i=1}^3 \Psi_m^i \int_{e_i} \left[\frac{\partial N_m^i}{\partial y} \frac{\partial N_L^i}{\partial x} - \frac{\partial N_m^i}{\partial x} \frac{\partial N_L^i}{\partial y} \right] d\Omega \\ = \int_{\Gamma_i} N_k^i \left[\frac{\partial \theta^i}{\partial x} nx + \frac{\partial \theta^i}{\partial y} ny \right] d\Gamma_i = W_k^i \quad (1, m, k = (1, 2, 3)) \end{aligned} \quad (28)$$

$$\sum_{i=1}^3 \int_{e_i} \frac{\partial N_k^i}{\partial x} \frac{\partial N_L^i}{\partial x} - \frac{\partial N_L^i}{\partial y} \frac{\partial N_k^i}{\partial y} - Sc \sum_{i=1}^3 \Psi_m^i \int_{e_i} \left[\frac{\partial N_m^i}{\partial y} \frac{\partial N_L^i}{\partial x} - \frac{\partial N_m^i}{\partial x} \frac{\partial N_L^i}{\partial y} \right]$$

$$= \int_{\Gamma_i} N_k^i \left[\left(\frac{\partial \theta^i}{\partial x} nx + \frac{\partial \theta^i}{\partial y} ny \right) \right] d\Gamma_i = W_k^i \quad (1, m, k = (1, 2, 3))$$

$$\sum_1 \int_{e_i} N^i \left(\frac{\partial N_k^i}{\partial x} \frac{\partial N_L^i}{\partial y} + \frac{\partial N_L^i}{\partial y} \frac{\partial N_k^i}{\partial x} \right) + \frac{2R}{\lambda} \Sigma \omega^i \int N_k^i N_L^i d\Omega - \frac{R}{\lambda} \Sigma \Psi^i \int \left(\frac{\partial N_k^i}{\partial x} \frac{\partial N_J^i}{\partial x} + \frac{\partial N_k^i}{\partial y} \frac{\partial N_J^i}{\partial y} \right) d\Omega$$

$$= \int_{\Gamma_i} N_k^i \left[\left(\frac{\partial \omega^i}{\partial x} - \frac{R}{\lambda} \frac{\partial \Psi^2}{\partial x} \right) nx + \left(\frac{\partial \omega^i}{\partial y} - \frac{R}{\lambda} \frac{\partial \Psi^2}{\partial y} \right) ny \right] d\Gamma_i = Q_i^N \quad (29)$$

Where $Q_k^i = Q_{k1}^i + Q_{k2}^i + Q_{k3}^i$, Q_k^i 's being the values of Q_k^i on the sides $s = (1, 2, 3)$ of the element e_i . The sign of Q_k^i 's depends on the direction of the outward normal with reference to the element.

Choosing different N_k^i 's as weight functions and following the same procedure we obtain matrix equations for three unknowns (Q_p^i)

$$(Q_p^i)(Q_p^i) = (Q_k^i) \quad (30)$$

Where (Q_{pk}^i) 3 x 3 a matrix is, $(Q_p^i), (Q^i)$ are column matrices?

Repeating the above process with each of s elements, we obtain sets of such matrix equations. Introducing the global coordinates and global values for (Q_p^i) and making use of inter element continuity and boundary conditions relevant to the problem the above stiffness matrices are assembled to obtain a global matrix equation. This global matrix is rxr square matrix if there are r distinct global nodes in the domain of flow considered.

Similarly substituting $\psi^i, \theta^i, \omega^i$ and ϕ^i in (16) and defining the error and following the Galerkin method we obtain using Green's Theorem, (6.3.10) reduces to

$$\int_{\Omega} \left[\frac{\partial N_k^i}{\partial x} \frac{\partial \Psi^i}{\partial x} + \frac{\partial N_k^i}{\partial y} \frac{\partial \Psi^i}{\partial y} + GD^{-1} \frac{\partial N_k^i}{\partial x} + \frac{RD^{-1}}{\lambda} \left(\frac{\partial N_k^i}{\partial x} \frac{\partial N^i}{\partial x} + \frac{\partial N_k^i}{\partial y} \frac{\partial N^i}{\partial y} \right) \right] d\Omega$$

$$= \int_{\Gamma} \left(\frac{\partial \Psi^i}{\partial x} nx + \frac{\partial \Psi^i}{\partial y} ny \right) d\Gamma + RD^{-1} \int_{\Gamma} N_k^i \left(\frac{\partial \omega^i}{\partial x} ny + \frac{\partial \omega^i}{\partial y} ny \right) d\Gamma = GD^{-1} \int_{\Gamma} N_k^i nxd\Gamma \quad (31)$$

In obtaining eqn (10) the Green's Theorem is applied with reference to derivatives of Ψ without affecting θ terms. Using eqn (20) in eqn (29) we have

$$\sum_m \Psi_m^i \left\{ \int_{\Omega} \left(\frac{\partial N_k^i}{\partial x} \frac{\partial N_m^i}{\partial x} + \frac{\partial N_m^i}{\partial y} \frac{\partial N_k^i}{\partial y} \right) d\Omega + GD^{-1} \left(\sum_L \theta_L^i \int_{\Omega} N_k^i (1 + 2rN^2_{k2}) \frac{\partial N_L^i}{\partial x} d\Omega \right) \right\}$$

$$= \int N_k^i \left[\left(\frac{\partial \Psi^i}{\partial x} + \frac{\partial N^i}{\partial x} \right) nx + \left(\frac{\partial \Psi^i}{\partial y} + \frac{\partial N^i}{\partial y} \right) ny \right] d\Gamma + \int N_k^i \theta^i d\Omega_i = \Gamma ki \quad (32)$$

In the problem under consideration, for computational purpose, we choose uniform mesh of 10 triangular elements. The domain has vertices whose global coordinates are (0, 0), (1, 0) and (1, c) in the non-dimensional form. Let e_1, e_2, \dots, e_{10} be the ten elements and let $\theta_1, \theta_2, \dots, \theta_{10}$ be the global values of θ , C_1, C_2, \dots, C_{10} be the global values of C and $\omega_1, \omega_2, \omega_3, \dots, \omega_{10}$ be the global values of ω and $\psi_1, \psi_2, \dots, \psi_{10}$ are the global values of ψ at the global nodes of the domain.

SHAPE FUNCTIONS AND STIFFNESS MATRICES

$$n_{1,1} = 1 - 3x$$

$$n_{2,2} = -1 + \frac{3y}{h}$$

$$n_{3,2} = -1 + 3x + \frac{3y}{h}$$

$$n_{4,2} = -2 + 3x$$

$$n_{5,2} = -1 + 3x - \frac{3y}{h}$$

$$n_{7,1} = 2 - \frac{3y}{h}$$

$$n_{8,1} = 3 - 3x$$

$$n_{9,3} = -1 + \frac{3y}{h}$$

$$n_{1,2} = 3x - \frac{3y}{h}$$

$$n_{2,3} = 1 - 3x + \frac{3y}{h}$$

$$n_{3,3} = -\frac{3y}{h}$$

$$n_{4,3} = 2 - 3x + \frac{3y}{h}$$

$$n_{5,3} = \frac{3y}{h}$$

$$n_{7,2} = -2 + 3x$$

$$n_{8,2} = -1 + 3x - \frac{3y}{h}$$

$$n_{2,1} = 1 - \frac{3y}{h}$$

$$n_{3,1} = 2 - 3x$$

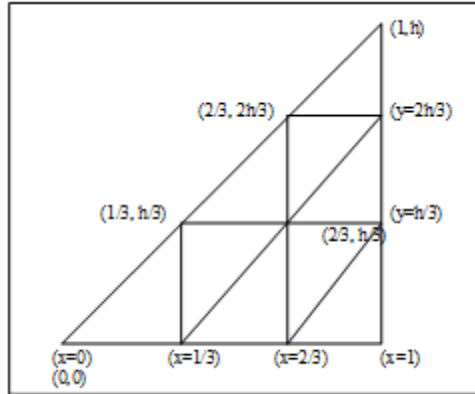
$$n_{4,1} = 1 - \frac{3y}{h}$$

$$n_{5,1} = 2 - 3x$$

$$n_{6,3} = 1 + \frac{3y}{h}$$

$$n_{7,3} = 1 - 3x + \frac{3y}{h}$$

$$n_{9,2} = 3x - \frac{3y}{h}$$



The global matrix for θ is

$$A_1 X_1 = B_1 \tag{33}$$

The global matrix for N is

$$A_2 X_2 = B_2 \tag{34}$$

The global matrix ψ is

$$A_3 X_3 = B_3 \tag{35}$$

The global matrix C is

$$A_4 X_4 = B_4 \tag{36}$$

Where

$$A_1 = \begin{bmatrix} -1 & 0 & 0 & 0 & 0 & 0 & \frac{-eR}{216} & 0 & 0 & 0 & 0 \\ 0 & -1 & 0 & 0 & 0 & \frac{-eR}{108} & \frac{-1}{e^2} + \frac{R}{27e^2} - \frac{R}{12e} & 0 & 0 & 0 & 0 \\ 0 & 0 & -1 & 0 & 0 & \frac{-1}{e^2} + \frac{R}{27e^2} - \frac{R}{36e} + \frac{eR}{18} & 0 & 0 & 0 & 0 & 0 \\ 0 & 0 & 0 & 0 & -1 & -2+C - \frac{R}{27} + \frac{R}{18C} + \frac{eR}{108} & 0 & 0 & 0 & 0 & 0 \\ 0 & 0 & 0 & 0 & 0 & 2 + \frac{1}{e^2} + \frac{1}{e} - \frac{2R}{27} - \frac{R}{27e^2} + \frac{R}{18e} - \frac{7eR}{27} & -2+C - \frac{R}{27} + \frac{R}{18C} + \frac{eR}{108} & \frac{-1}{e^2} + \frac{R}{27e^2} - \frac{R}{36e} + \frac{eR}{18} & 0 & 0 & 0 \\ 0 & 0 & 0 & 0 & 0 & -C + \frac{11eR}{108} & \frac{1}{e} + C - \frac{35eR}{108} & \frac{19eR}{216} & 0 & 0 & 0 \\ 0 & 0 & 0 & 0 & 0 & \frac{-1}{e} + \frac{5eR}{108} & \frac{11eR}{216} & \frac{1}{e} + C - \frac{37eR}{108} & 0 & 0 & 0 \\ 0 & 0 & 0 & 0 & -1 & 0 & 0 & 0 & 0 & 0 & 0 \\ 0 & 0 & 0 & 0 & 0 & \frac{R}{9} - \frac{R}{36e} - \frac{eR}{54} & 0 & -2+C - \frac{7R}{27} + \frac{R}{9e} + \frac{11eR}{108} & -1 & 0 & 0 \\ 0 & 0 & 0 & 0 & 0 & 0 & 0 & \frac{eR}{8} & 0 & -1 & 0 \end{bmatrix}$$

$$A_2 = \begin{bmatrix} -1 & e_{21} & 0 & 0 & 0 & 0 & e_{71} & 0 & 0 & 0 & 0 \\ 0 & e_{22} & e_{23} & 0 & 0 & e_{26} & e_{27} & 0 & 0 & 0 & 0 \\ 0 & e_{32} & e_{33} & 0 & 0 & e_{36} & 0 & 0 & 0 & 0 & 0 \\ 0 & 0 & e_{43} & -1 & 0 & 0 & 0 & 0 & 0 & 0 & 0 \\ 0 & 0 & e_{53} & 0 & e_{55} & e_{56} & 0 & 0 & 0 & 0 & 0 \\ 0 & e_{62} & e_{63} & 0 & 0 & e_{66} & e_{67} & e_{68} & 0 & 0 & 0 \\ 0 & e_{72} & 0 & 0 & 0 & -c & e_{77} & e_{78} & 0 & 0 & 0 \\ 0 & 0 & 0 & 0 & 0 & e_{86} & e_{87} & e_{88} & 0 & 0 & 0 \\ 0 & 0 & 0 & 0 & 0 & e_{96} & 0 & e_{98} & -1 & 0 & 0 \\ 0 & 0 & 0 & 0 & 0 & 0 & 0 & -\frac{p\Psi_8}{2} & 0 & -1 & 0 \end{bmatrix}$$

$$A_3 = \begin{bmatrix} -1 & \frac{-a}{2} & 0 & 0 & 0 & 0 & 0 & 0 & 0 & 0 & 0 \\ -1 + \frac{a}{2} & 1 + \frac{1}{e^2} & \frac{-a}{2} & 0 & 0 & 0 & 0 & \frac{-1}{e^2} & 0 & 0 & 0 \\ 0 & -1 + \frac{a}{2} & 1 + \frac{1}{e^2} & \frac{-a}{2} & 0 & 0 & 0 & \frac{-1}{e^2} & 0 & 0 & 0 \\ 0 & 0 & \frac{18e^2 - 9e^3}{18e^2} & \frac{18 + 9e - 9e^3}{18e^2} & \frac{-18e^2 - 9e^3}{18e^2} & 0 & 0 & 0 & 0 & 0 & 0 \\ 0 & 0 & 0 & \frac{-a}{2} & 0 & 0 & 2 + \frac{1}{e^2} & -2 + C & 0 & 0 & 0 \\ 0 & 0 & \frac{-a}{2} & 0 & 0 & 0 & -1 + \frac{a}{2} & \frac{1}{e} + C & \frac{e}{6} & 0 & 0 \\ 0 & 0 & 0 & 0 & 0 & 0 & \frac{-1}{e} & \frac{11eR}{216} & C - a & 0 & 0 \\ 0 & 0 & 0 & 0 & 0 & -1 & 0 & 0 & 0 & 0 & 0 \\ 0 & 0 & 0 & 0 & 0 & 0 & 0 & 0 & -a & -1 & 0 \\ 0 & 0 & 0 & 0 & 0 & 0 & 0 & 0 & \frac{e}{8} & 0 & -1 \end{bmatrix}$$

$$B_1 = \begin{pmatrix} b_{11} \\ b_{21} \\ b_{31} \\ b_{41} \\ b_{51} \\ b_{61} \\ b_{71} \\ b_{81} \\ b_{91} \\ b_{101} \end{pmatrix}, \quad B_1 = \begin{pmatrix} d_{11} \\ d_{21} \\ d_{31} \\ d_{41} \\ d_{51} \\ d_{61} \\ d_{71} \\ d_{81} \\ d_{91} \\ d_{101} \end{pmatrix}$$

Similarly A₄ and B₃ matrices.

The domain consist two horizontal levels and the solution for Ψ, θ, C and ω at each level may be expressed in terms of the nodal values as follows,

In the horizontal strip $0 \leq y \leq \frac{h}{3}$

$$\Psi = (\Psi_1 N^1_1 + \Psi_2 N^1_2 + \Psi_7 N^1_7) H(1 - \tau_1) \\ = \Psi_1 (1-4x) + \Psi_2 4(x - \frac{y}{h}) + \Psi_7 (\frac{4y}{h} (1 - \tau_1)) \quad \left(0 \leq x \leq \frac{1}{3}\right)$$

$$\Psi = (\Psi_2 N^2_2 + \Psi_3 N^2_3 + \Psi_6 N^2_6) H(1 - \tau_2) + (\Psi_2 N^2_2 + \Psi_7 N^2_7 + \Psi_6 N^2_6) H(1 - \tau_3) \quad \left(\frac{1}{3} \leq x \leq \frac{2}{3}\right) \\ = (\Psi_2 2(1-2x) + \Psi_3 (4x - \frac{4y}{h} - 1) + \Psi_6 (\frac{4y}{h})) H(1 - \tau_2) + (\Psi_2 (1 - \frac{4y}{h}) + \Psi_7 (1 + \frac{4y}{h} - 4x) + \Psi_6 (4x - 1)) H(1 - \tau_3)$$

$$\Psi = (\Psi_3 N^3_3 + \Psi_4 N^3_4 + \Psi_5 N^3_5) H(1 - \tau_3) + (\Psi_3 N^4_3 + \Psi_5 N^4_5 + \Psi_6 N^4_6) H(1 - \tau_4) \quad \left(\frac{2}{3} \leq x \leq 1\right) \\ = (\Psi_3 (3-4x) + \Psi_4 2(2x - \frac{2y}{h} - 1) + \Psi_6 (\frac{4y}{h} - 4x + 3)) H(1 - \tau_3) + \Psi_3 (1 - \frac{4y}{h}) + \Psi_5 (4x - 3) + \Psi_6 (\frac{4y}{h}) H(1 - \tau_4)$$

Along the strip $\frac{h}{3} \leq y \leq \frac{2h}{3}$

$$\Psi = (\Psi_7 N^6_7 + \Psi_6 N^6_6 + \Psi_8 N^6_8) H(1 - \tau_2) \quad \left(\frac{1}{3} \leq x \leq 1\right) \\ + (\Psi_6 N^7_6 + \Psi_9 N^7_9 + \Psi_8 N^7_8) H(1 - \tau_3) + (\Psi_6 N^8_6 + \Psi_5 N^8_5 + \Psi_9 N^8_9) H(1 - \tau_4)$$

$$\Psi = (\Psi_7 2(1-2x) + \Psi_6 (4x-3) + \Psi_8 (\frac{4y}{h} - 1)) H(1 - \tau_3) \\ + \Psi_6 (2(1 - \frac{2y}{h}) + \Psi_9 (\frac{4y}{h} - 1) + \Psi_8 (1 + \frac{4y}{h} - 4x)) H(1 - \tau_4) \\ + \Psi_6 (4(1-x) + \Psi_5 (4x - \frac{4y}{h} - 1) + \Psi_9 2(\frac{2y}{h} - 1)) H(1 - \tau_5)$$

Along the strip $\frac{2h}{3} \leq y \leq 1$

$$\Psi = (\Psi_8 N^9_8 + \Psi_9 N^9_9 + \Psi_{10} N^9_{10}) H(1 - \tau_6) \quad \left(\frac{2}{3} \leq x \leq 1\right) \\ = \Psi_8 (4(1-x) + \Psi_9 4(x - \frac{y}{h}) + \Psi_{10} 2(\frac{4y}{h} - 3)) H(1 - \tau_6)$$

where $\tau_1 = 4x$, $\tau_2 = 2x$, $\tau_3 = \frac{4x}{3}$,
 $\tau_4 = 4(x - \frac{y}{h})$, $\tau_5 = 2(x - \frac{y}{h})$, $\tau_6 = \frac{4}{3}(x - \frac{y}{h})$

And H represents the Heaviside function.

The expressions for θ are

In the horizontal strip $0 \leq y \leq \frac{h}{3}$

$$\theta = \theta_1(1-4x) + \theta_2 4(x - \frac{y}{h}) + \theta_7 (\frac{4y}{h}) H(1 - \tau_1) \quad \left(0 \leq x \leq \frac{1}{3}\right)$$

$$\theta = \theta_2(2(1-2x) + \theta_3(4x - \frac{4y}{c} - 1) + \theta_6(\frac{4y}{c})) H(1 - \tau_2) \\ + \theta_2(1 - \frac{4y}{h}) + \theta_7(1 + \frac{4y}{h} - 4x) + \theta_6(4x - 1) H(1 - \tau_3) \quad \left(\frac{1}{3} \leq x \leq \frac{2}{3}\right)$$

$$\theta = \theta_3(3-4x) + 2\theta_4(2x - \frac{2y}{h} - 1) + \theta_6(\frac{4y}{h} - 4x + 3) H(1 - \tau_3) \\ + (\theta_3(1 - \frac{4y}{h}) + \theta_5(4x - 3) + \theta_6(\frac{4y}{h})) H(1 - \tau_4) \quad \left(\frac{2}{3} \leq x \leq 1\right)$$

Along the strip $\frac{h}{3} \leq y \leq \frac{2h}{3}$

$$\theta = \theta_7(2(1-2x) + \theta_6(4x - 3) + \theta_8(\frac{4y}{h} - 1)) H(1 - \tau_3) \quad \left(\frac{1}{3} \leq x \leq \frac{2}{3}\right)$$

$$+ (\theta_6(2(1 - \frac{2y}{h}) + \theta_9(\frac{4y}{h} - 1) + \theta_8(1 + \frac{4y}{h} - 4x)) H(1 - \tau_4)$$

$$+ (\theta_6(4(1-x) + \theta_5(4x - \frac{4y}{h} - 1) + \theta_9(2(\frac{4y}{h} - 1))) H(1 - \tau_5)$$

Along the strip $\frac{2h}{3} \leq y \leq 1$

$$\theta = (\theta_8(4(1-x) + \theta_9(4x - \frac{y}{h}) + \theta_{10}(\frac{4y}{h} - 3)) H(1 - \tau_6) \quad \left(\frac{2}{3} \leq x \leq 1\right)$$

The expressions for C are

In the horizontal strip $0 \leq y \leq \frac{h}{3}$

$$C = [C_1(1-4x) + C_2 4(x - \frac{y}{h}) + C_7 (\frac{4y}{h}) H(1 - \tau_1) \quad \left(0 \leq x \leq \frac{1}{3}\right)$$

$$C = (C_2(2(1-2x) + C_3(4x - \frac{4y}{c} - 1) + C_6(\frac{4y}{c})) H(1 - \tau_2) \\ + C_2(1 - \frac{4y}{h}) + C_7(1 + \frac{4y}{h} - 4x) + C_6(4x - 1) H(1 - \tau_3) \quad \left(\frac{1}{3} \leq x \leq \frac{2}{3}\right)$$

$$C = C_3(3-4x) + 2C_4(2x - \frac{2y}{h} - 1) + C_6(\frac{4y}{h} - 4x + 3) H(1 - \tau_3) \\ + (C_3(1 - \frac{4y}{h}) + C_5(4x - 3) + C_6(\frac{4y}{h})) H(1 - \tau_4) \quad \left(\frac{2}{3} \leq x \leq 1\right)$$

Along the strip $\frac{h}{3} \leq y \leq \frac{2h}{3}$

$$C = (C_7(2(1-2x) + C_6(4x-3) + C_8(\frac{4y}{h} - 1)) H(1 - \tau_3) \quad \left(\frac{1}{3} \leq x \leq \frac{2}{3}\right)$$

$$+ (C_6(2(1 - \frac{2y}{h}) + C_9(\frac{4y}{h} - 1) + C_8(1 + \frac{4y}{h} - 4x)) H(1 - \tau_4)$$

$$+ (\theta_6(4(1-x) + \theta_5(4x - \frac{4y}{h} - 1) + \theta_9 2(\frac{4y}{h} - 1)) H(1 - \tau_5)$$

Along the strip $\frac{2h}{3} \leq y \leq 1$

$$C = (C_8 4(1-x) + C_9 4(x - \frac{y}{h}) + C_{10}(\frac{4y}{h} - 3) H(1 - \tau_6) \quad \left(\frac{2}{3} \leq x \leq 1\right)$$

The expressions for ω are

$$\omega = [\omega_1(1-4x) + \omega_2 4(x - \frac{y}{c}) + \omega_7 (\frac{4y}{c})] H(1 - \tau_1) \quad \left(0 \leq x \leq \frac{1}{3}\right)$$

$$\omega = (\omega_2(2(1-2x) + \omega_3 (4x - \frac{4y}{h} - 1) + \omega_6(\frac{4y}{h})) H(1 - \tau_2)$$

$$+ \omega_2(1 - \frac{4y}{h}) + \omega_7(1 + \frac{4y}{h} - 4x) + \omega_6(4x - 1) H(1 - \tau_3) \quad \left(\frac{1}{3} \leq x \leq \frac{2}{3}\right)$$

$$\omega = \omega_3(3-4x) + 2 \omega_4(2x - \frac{2y}{h} - 1) + \omega_6(\frac{4y}{h} - 4x + 3) H(1 - \tau_3)$$

$$+ (\omega_3(1 - \frac{4y}{h}) + \omega_5(4x-3) + \omega_6(\frac{4y}{h})) H(1 - \tau_4) \quad \left(\frac{2}{3} \leq x \leq 1\right)$$

Along the strip $\frac{h}{3} \leq y \leq \frac{2h}{3}$

$$\omega = (\omega_7(2(1-2x) + \omega_6(4x-3) + \omega_8(\frac{4y}{c} - 1)) H(1 - \tau_3) \quad \left(\frac{1}{3} \leq x \leq \frac{2}{3}\right)$$

$$+ (\omega_6(2(1 - \frac{2y}{h}) + \omega_9(\frac{4y}{h} - 1) + \omega_8(1 + \frac{4y}{h} - 4x)) H(1 - \tau_4)$$

$$+ (\omega_6(4(1-x) + \omega_5(4x - \frac{4y}{h} - 1) + \omega_9 2(\frac{4y}{h} - 1)) H(1 - \tau_5)$$

Along the strip $\frac{2h}{3} \leq y \leq 1$

$$\omega = (\omega_8 4(1-x) + \omega_9 4(x - \frac{y}{h}) + \omega_{10}(\frac{4y}{h} - 3) H(1 - \tau_6) \quad \left(\frac{2}{3} \leq x \leq 1\right)$$

The dimensionless Nusselt numbers on the non-insulated boundary walls of the rectangular duct are calculated using the formula

$$Nu = \left(\frac{\partial \theta}{\partial x}\right)_{x=1}$$

$$Sh = \left(\frac{\partial C}{\partial x}\right)_{x=1}$$

$$Cw = \left(\frac{\partial \omega}{\partial x}\right)_{x=1}$$

Nusselt number on the side wall $x=1$ in the different regions are

$$\begin{aligned} \text{Nu}_1 = 2-4 \theta_3, \quad \text{Sh}_1 = 2-4 C_3, \quad (C_w)_1 = 2 - 4\omega_3 & \quad 0 \leq y \leq \frac{h}{3} \\ \text{Nu}_2 = 2-4 \theta_6, \quad \text{Sh}_2 = 2-4 C_6, \quad (C_w)_2 = 2 - 4\omega_3 & \quad \frac{h}{3} \leq y \leq 2 \frac{h}{3} \\ \text{Nu}_3 = 2-4 \theta_9, \quad \text{Sh}_3 = 2-4 C_9, \quad (C_w)_3 = 2 - 4\omega_3 & \quad \frac{2h}{3} \leq y \leq 1 \end{aligned}$$

The details of a_{11} , b_{11} , a_{r1} , b_{r1} , c_{r1} etc., are shown in appendix.

The equilibrium conditions are

$$\begin{aligned} R_3^1 + R_1^2 = 0, \quad R_3^2 + R_1^3 = 0 \quad R_3^3 + R_1^4 = 0, \quad R_3^4 + R_1^5 = 0 \\ Q_3^1 + Q_1^2 = 0, \quad Q_3^2 + Q_1^3 = 0 \quad Q_3^3 + Q_1^4 = 0, \quad Q_3^4 + Q_1^5 = 0 \\ S_3^1 + S_1^2 = 0, \quad S_3^2 + S_1^3 = 0 \quad S_3^3 + S_1^4 = 0, \quad S_3^4 + S_1^5 = 0 \end{aligned} \quad (37)$$

Solving these coupled global matrices for temperature, micro concentration and velocity equations (33–37) respectively and using the iteration procedure we determine the unknown global nodes through which the temperature, micro rotation and velocity of different intervals at any arbitrary axial cross section are obtained.

4. RESULTS AND DISCUSSION

In this analysis, we investigate the effect of non linear density temperature on convective heat and mass transfer flow of a micropolar fluid in a rectangular duct. The equations governing the flow of heat and mass transfer are non linear coupled equations. It is not possible to find closed form solutions; therefore we solve these equations by using Galerkin finite element analysis with three noded triangular elements. The temperature, concentration, angular velocity have been analyzed for different values Grashof number (G), Darcy parameter (D^{-1}), Buoyancy ratio (N), Micropolar parameter (R), Schmidt number (Sc), Density ratio (γ), Prandtl number (P).

The temperature distribution (θ) is exhibited in figs (3-18) for different values G, D^{-1} , N, R, γ and P at horizontal levels $Y = h/3$ and $Y=2h/3$ and vertical levels $X=1/3$ and $2/3$. We follow the convention that the non - dimensional temperature (θ) is Positive or negative according as the actual temperature (T) is greater or lesser than T_c , the temperature on cold wall. From figs (3-6) we find that an increase in the Grashof number (G) enhances the actual temperature at $Y=2h/3$ and $x=1/3$ levels while at the levels $y=h/3$ and $x=2/3$, the actual temperature enhances with increase in $G \leq 3 \times 10^2$ and reduces with higher $G \geq 5 \times 10^2$. The variation of θ with D^{-1} shows that lesser the permeability of the porous medium ($D^{-1} \leq 10$) larger the actual temperature at $Y=h/3, 2h/3$ and $X= 2/3$ levels and smaller at $X=1/3$ level, for further lowering of the permeability larger the actual temperature at $Y=2h/3$ and $x=1/3$ levels and smaller at $Y=h/3$ and $x=2/3$ levels. The variation of θ with buoyancy ratio (N) is exhibited in figs (7-10) for different levels. It is found that when the molecular buoyancy force dominates over the thermal buoyancy force the actual temperature reduces at all the levels when the buoyancy forces are in the same direction and for the forces acting in opposite direction, the actual temperature enhances at both horizontal levels and vertical level $X=2/3$ and while at the vertical level $X=1/3$, it reduces in the flow of region. Figs (11-14) represent the variation of θ with Micropolar parameter (R). It is found that an increase in $R \leq 200$, reduces the actual temperature and enhances with higher $R \geq 300$ at $Y=h/3$, $Y=2h/3$ and $X=2/3$ levels. At $X=1/3$ level, the actual temperature enhances with lower and higher values of R and reduces with intermediate value of $R = 200$. Figs (15-18) represent of θ with density ratio (γ) shows that an increase in $\gamma \leq 0.03$ reduces the actual temperature and enhances at higher values of $\gamma \geq 0.05$ at $y=h/3, 2h/3$ and $x=1/3$ levels. At $x=2/3$ level, the actual temperature reduces in the horizontal strip except in the region ($0 \leq y \leq 0.132$) enhances with higher $\gamma=0.05$ and again reduces for still higher at $\gamma=0.07$ (Figs.15-18). The variation of θ with prandtl number (Pr) shows that lesser the thermal conductivity smaller the actual temperature at $y=2h/3$ and $x=1/3$ levels and larger at $y=h/3$ at $x=2/3$ levels.

The non-dimensional concentration distribution (C) is shown in figs (19-34) for different parametric values at different horizontal and vertical levels. We follow the actual concentration enhances with $G \leq 3 \times 10^2$ and reduces with $G \geq 5 \times 10^2$ at both horizontal levels. At $x=1/3$ level it enhances with G. At higher vertical level $x=2/3$ level, the actual concentration enhances in the horizontal strip (0.132,0.066) and reduces in the region (0,0.66) with increase in G and the reversed effect is noticed in the behavior of the actual concentration in the above horizontal strip with higher $G=5$. Figs (23-26) represent the concentration with buoyancy ratio (N). It is found that when the molecular buoyancy force dominates over the thermal buoyancy force the actual concentration reduces at $y=h/3$ and $x=1/3$ levels irrespective of the directions of buoyancy forces. At $y=2h/3$ and $x=2/3$ levels, the actual concentration reduces with increase in $N > 0$ and enhances with increase $|N| (=0)$. Figs 27-30 represent the variation of C with micro polar parameter (R). It is found that the actual concentration reduces with increase in $R \leq 100$ and enhances with higher $R \geq 200$. At $y=h/3, 2h/3$ and $x=2/3$ levels, while at $x = 1/3$ level the actual concentration enhances with $R \leq 200$ and reduces with higher $R \geq 300$. Figs (31-34) represent the variation of C with density ratio (γ). It is found that at $y=h/3, 2h/3$ and $x=2/3$

levels, the actual concentration enhances with $\gamma=0.03$ and reduces for higher $\gamma = 0.03$ and again enhances for still higher $\gamma = 0.07$. The variation of C with Prandtl number (Pr) is exhibited in Figs (31-34) at different levels. It is found the actual concentration reduces at both horizontal levels and $x=1/3$ level and enhances at higher vertical level $x=2/3$.

Figs (35-50) represent the variation of angular velocity (ω) for different parametric values at different levels. Figs (35-38) represent the variation of angular velocity with G and D^{-1} . It is found that at $y=h/3, 2h/3$ and $x=2/3$ levels the angular velocity enhances with $G \leq 3 \times 10^2$ and reduces with higher $G \geq 5 \times 10^2$ at all levels. The variation of ω with D^{-1} shows that the angular velocity enhances with D^{-1} at $y=2h/3$ and $x=1/3$ levels, at $y=2/3$ it enhances with $D^{-1} \leq 10$ and reduces with $D^{-1} \geq 1.5$. At $x=2/3$, the angular velocity enhances in the horizontal strip (0, 0.33) and reduces in the region (0.396, 0.66) (Figs 35-38). The variation of ω with buoyancy ratio (N), we find that when the molecular buoyancy force dominates over the thermal buoyancy force, $|\omega|$ enhances at both horizontal levels and at $x=1/3$ level irrespective of the directions of the buoyancy forces, while at $x=2/3$ level it enhances with $N > 0$ and an increase in $|N|$ reduces $|\omega|$ in the horizontal strip (0, 0.033) and enhances in the region (0.396, 0.66) (Figs 39-42). The variation of ω with R shows that at $y=2h/3$ level, $|\omega|$ reduces with $R \leq 100$ and enhances with $R \geq 200$. At $x=1/3$ level, $|\omega|$ enhances with $R \leq 100$, reduces with higher $R=0.2$ and again enhances with higher $R=300$. At $y=h/3$ level, an increase in $R \leq 100$ enhances $|\omega|$ in the vertical strip (0.033, 0.663) and reduces in the region (0.729, 0.927) while for higher $R \geq 200$ $|\omega|$ reduces in the region (0.333, 0.663) and enhances in the region (0.729, 0.927). At $x=2/3$ level $|\omega|$ reduces with $R \leq 100$ and for higher $R \geq 200$, we notice an enhancement in $|\omega|$ in the region (0.066, 0.33) and reduces in the region (0.396, 0.66) and for higher $R \geq 300$, $|\omega|$ enhances in the entire horizontal strip (0, 0.66) (Fig. 43-46). Figs (47-50) represent the variation of ω with Prandtl number (P) shows that $|\omega|$ reduces with increase in P at $y=h/3$ and $x=1/3$ levels and enhances at $y=2h/3$ and $x=2/3$ levels. The variation of ω with density ratio (γ) shows that an increase in the density ratio ≤ 0.03 , enhances $|\omega|$ at $y=h/3$ and reduces at $x=1/3$ level and for higher $\gamma \geq 0.05$, $|\omega|$ reduces at $y=h/3$ level and enhances at $x=1/3$ level at $x=2h/3$ level, $|\omega|$ reduces with increase in $\gamma \leq 0.05$ and enhances with higher $\gamma \geq 0.07$ at $x=2/3$ level an increase in $\gamma \leq 0.03$ enhances the $|\omega|$ in the horizontal strip (0.066, 0.33) and reduces in the strip (0.396, 0.66) and higher $\gamma \geq 0.05$ we notice an enhancement in $|\omega|$.

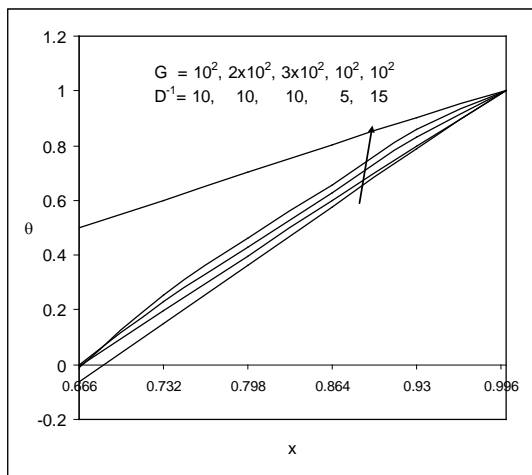


Fig. 3 : Variation of θ with G, D^{-1} at $y = \frac{2h}{3}$ level

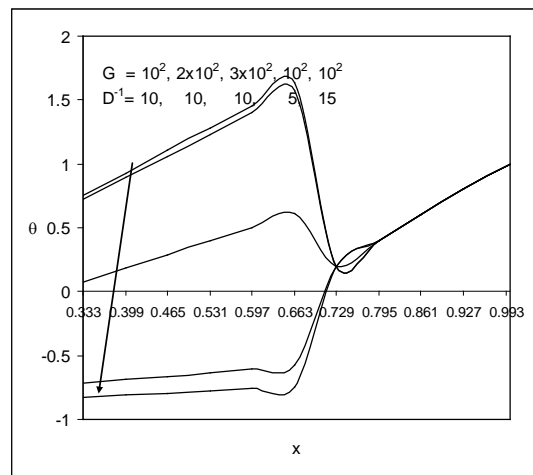


Fig. 4 : Variation of θ with G, D^{-1} at $y = \frac{h}{3}$ level

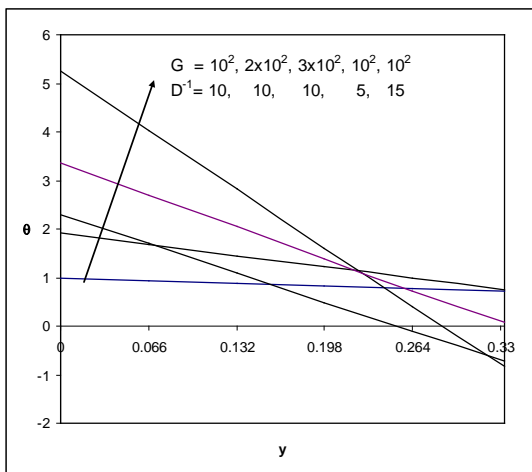


Fig. 5 : Variation of θ with G, D^{-1} at $x = \frac{1}{3}$ level

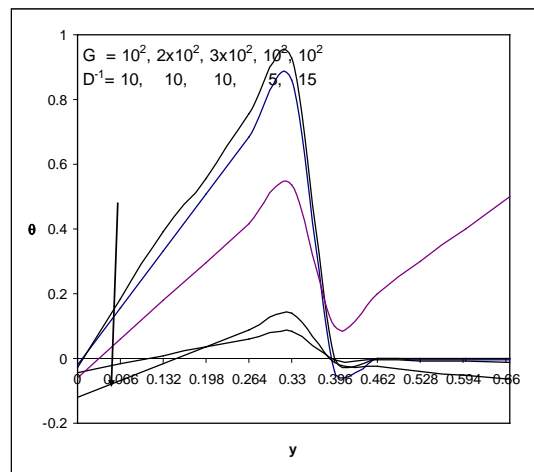


Fig. 6 : Variation of θ with G, D^{-1} at $x = \frac{2}{3}$ level

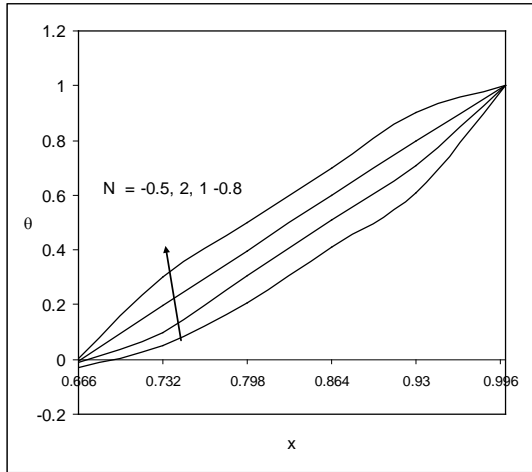


Fig. 7 : Variation of θ with N at $y = \frac{2h}{3}$ level

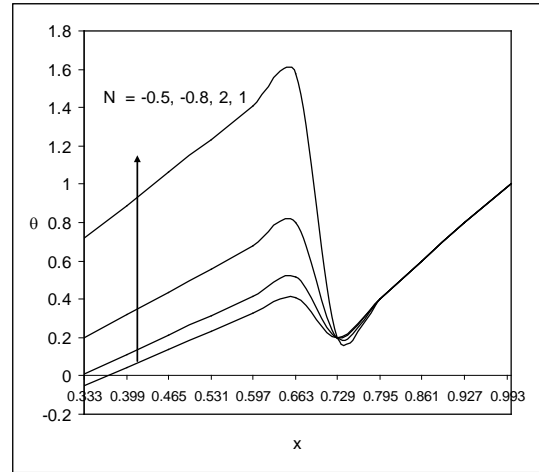


Fig. 8 : Variation of θ with N at $y = \frac{h}{3}$ level

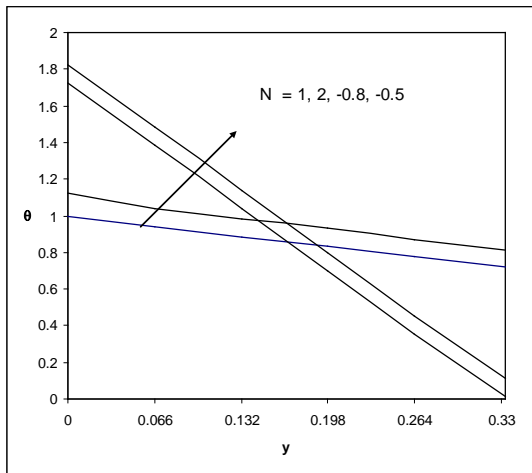


Fig. 9 : Variation of θ with N at $x = \frac{1}{3}$ level

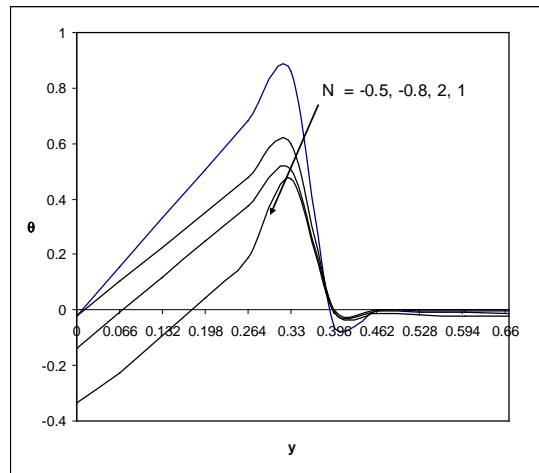


Fig. 10 : Variation of θ with N at $x = \frac{2}{3}$ level

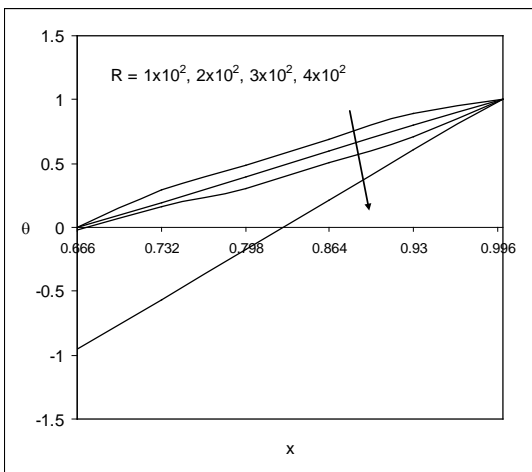


Fig. 11 : Variation of θ with R at $y = \frac{2h}{3}$ level

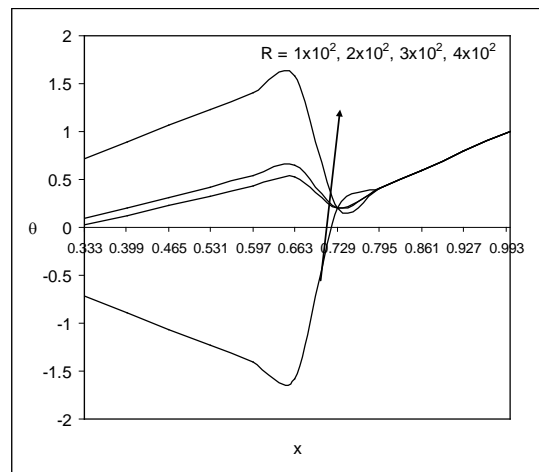


Fig. 12 : Variation of θ with R at $y = \frac{h}{3}$ level

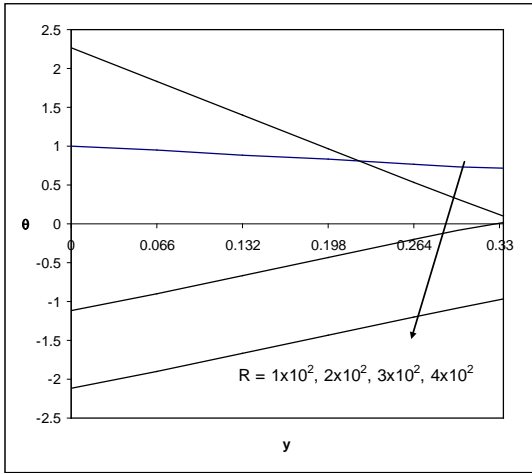


Fig. 13: Variation of θ with R at $x = \frac{1}{3}$ level

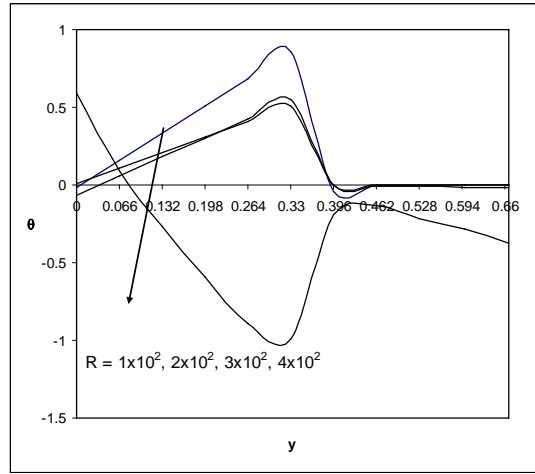


Fig. 14: Variation of θ with R at $x = \frac{2}{3}$ level

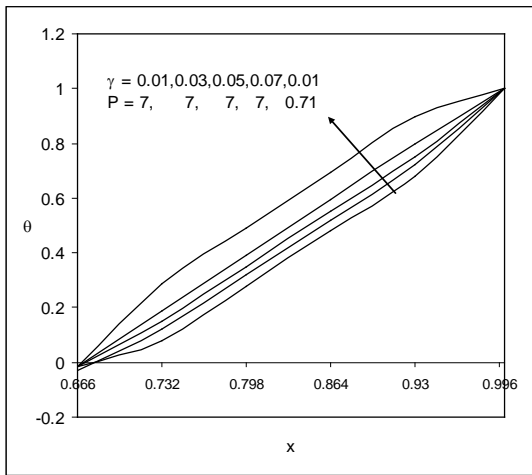


Fig. 15: Variation of θ with γ, P at $y = \frac{2h}{3}$ level

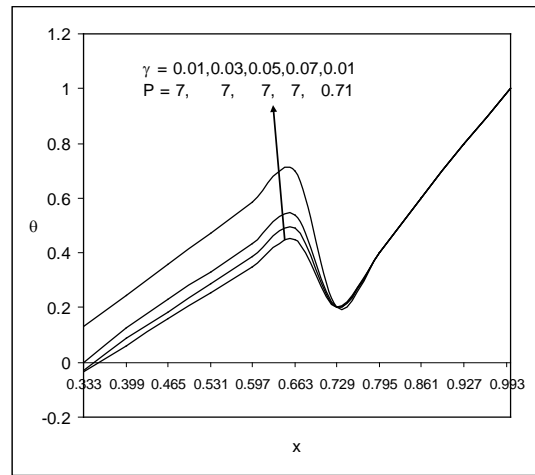


Fig. 16: Variation of θ with γ, P at $y = \frac{h}{3}$ level

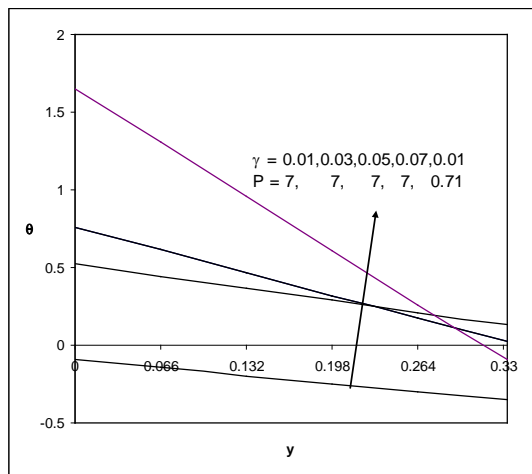


Fig. 17: Variation of θ with γ, P at $x = \frac{1}{3}$ level

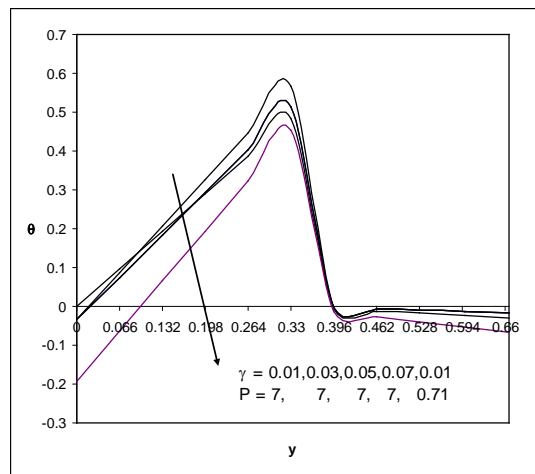


Fig. 18: Variation of θ with γ, P at $x = \frac{2}{3}$ level

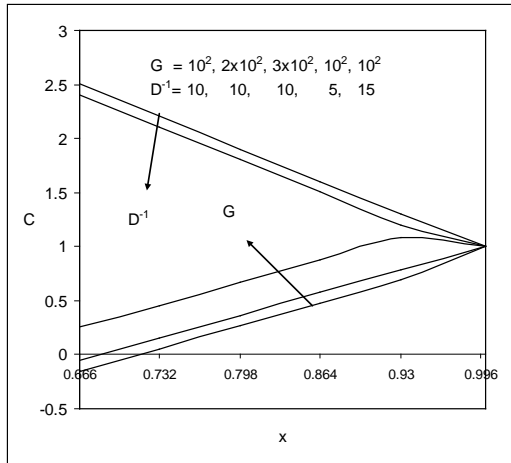


Fig. 19 : Variation of C with G, D^{-1} at $y = \frac{2h}{3}$ level

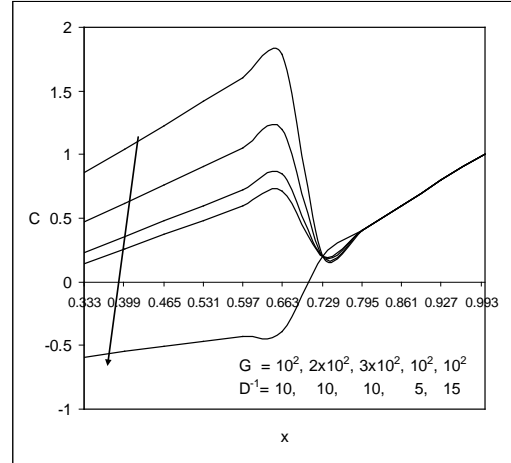


Fig. 20 : Variation of C with G, D^{-1} at $y = \frac{h}{3}$ level

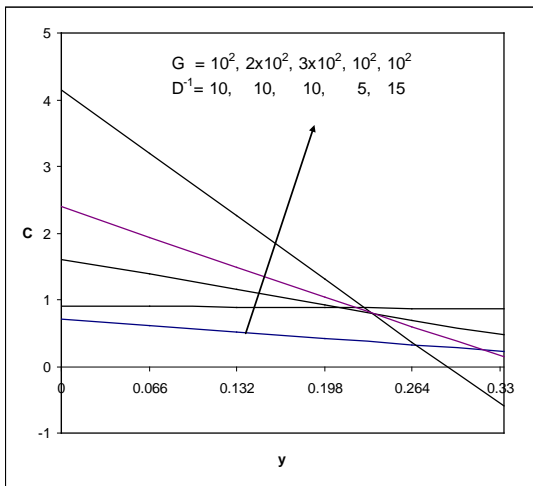


Fig. 21 : Variation of C with G, D^{-1} at $x = \frac{1}{3}$ level

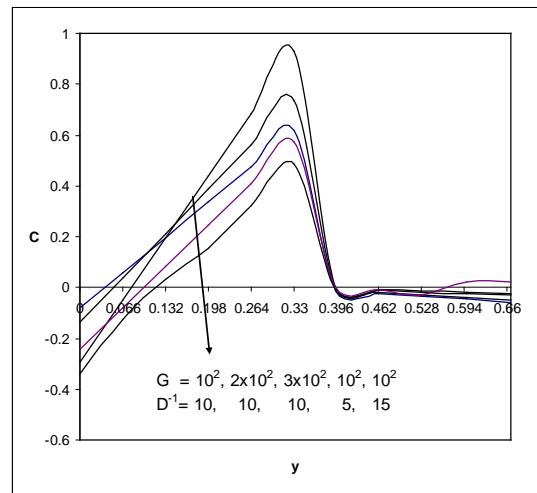


Fig. 22 : Variation of C with G, D^{-1} at $x = \frac{2}{3}$ level

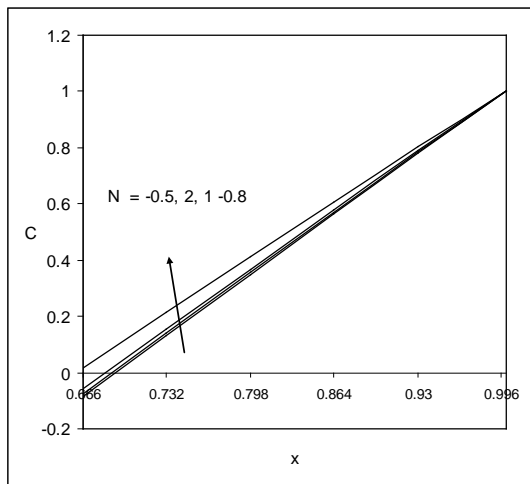


Fig. 23: Variation of C with N at $y = \frac{2h}{3}$ level

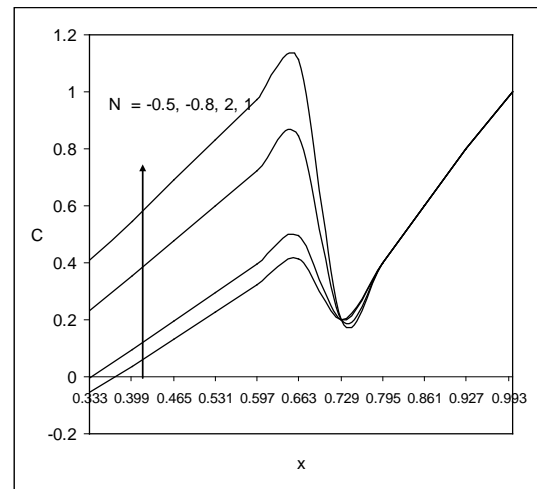


Fig. 24 : Variation of C with N at $y = \frac{h}{3}$ level

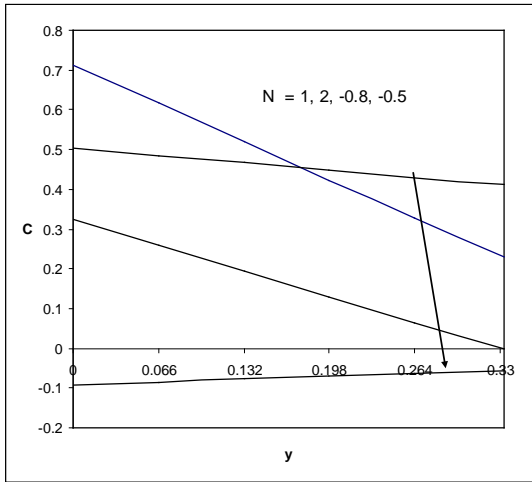


Fig. 25 : Variation of C with N at $x = \frac{1}{3}$ level

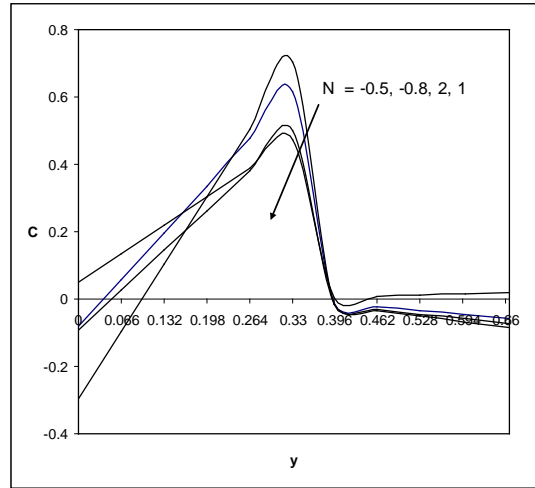


Fig. 26 : Variation of C with N at $x = \frac{2}{3}$ level

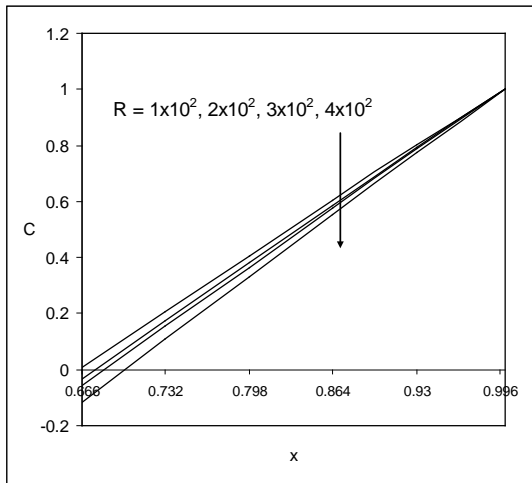


Fig. 27 : Variation of C with R at $y = \frac{2h}{3}$ level

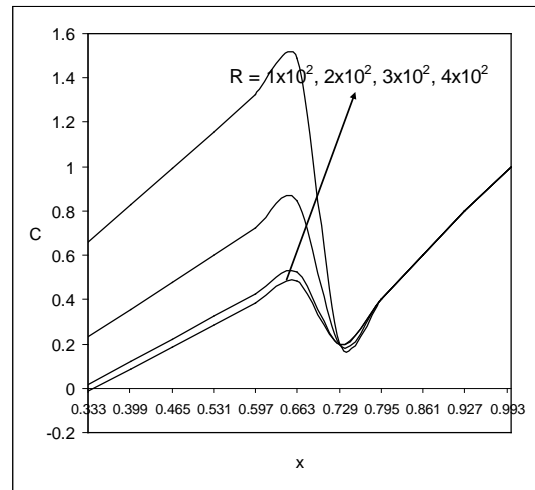


Fig. 28 : Variation of C with R at $y = \frac{h}{3}$ level

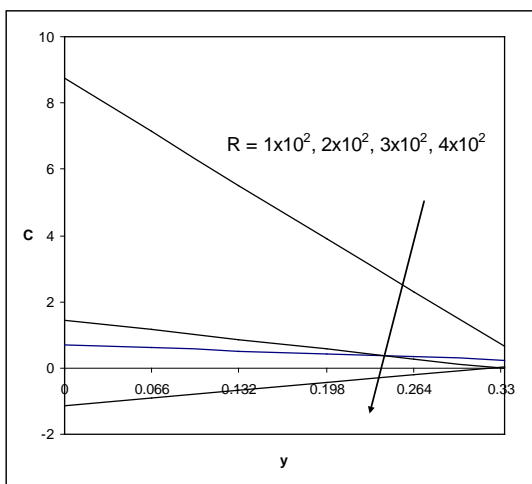


Fig. 29 : Variation of C with R at $x = \frac{1}{3}$ level

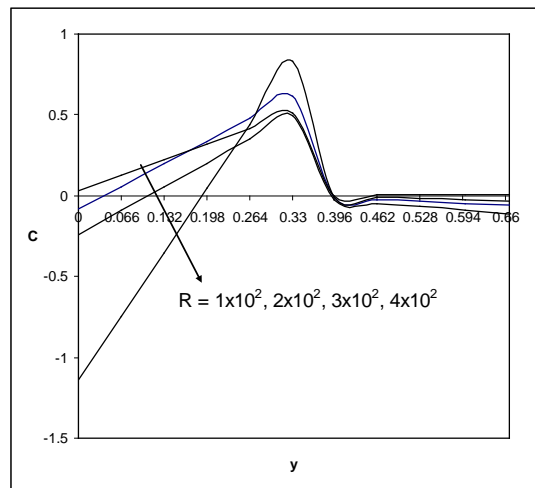


Fig. 30 : Variation of C with R at $x = \frac{2}{3}$ level

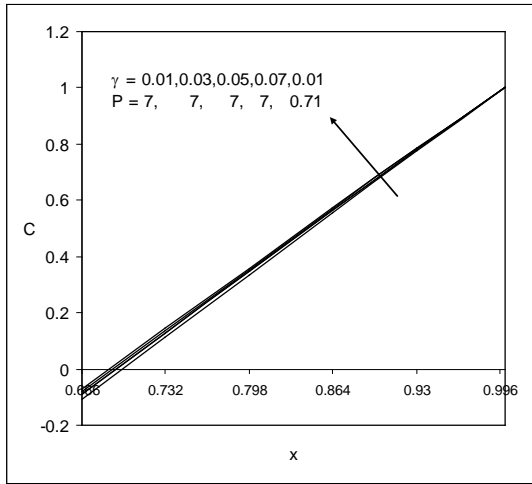


Fig. 31 : Variation of C with γ, P at $y = \frac{2h}{3}$ level

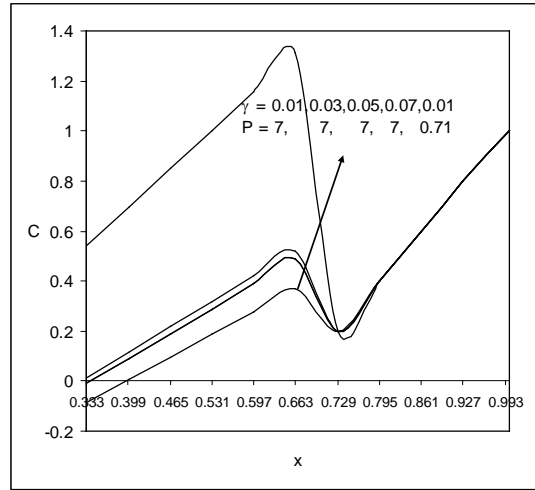


Fig. 32 : Variation of C with γ, P at $y = \frac{h}{3}$ level

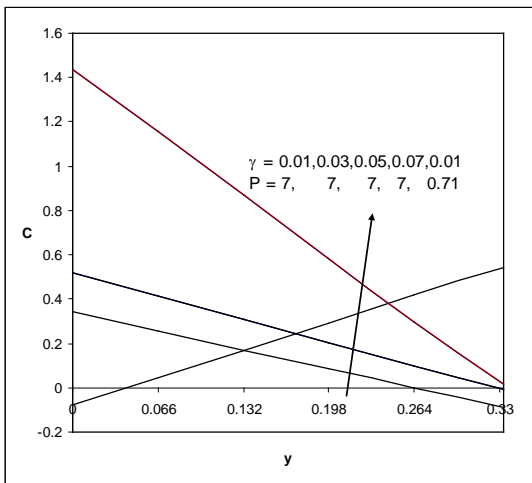


Fig. 33 : Variation of C with γ, P at $x = \frac{1}{3}$ level

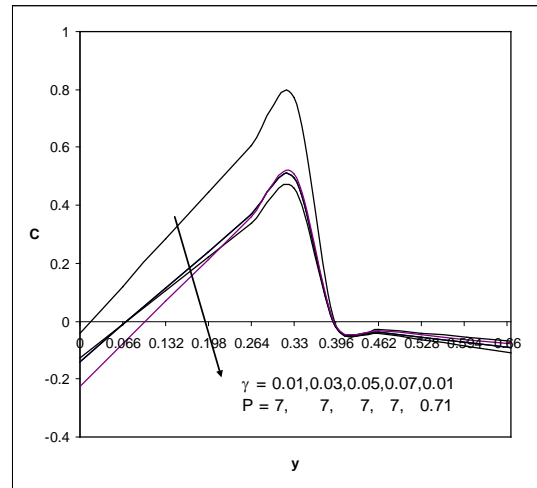


Fig. 34 : Variation of C with γ, P at $x = \frac{2}{3}$ level

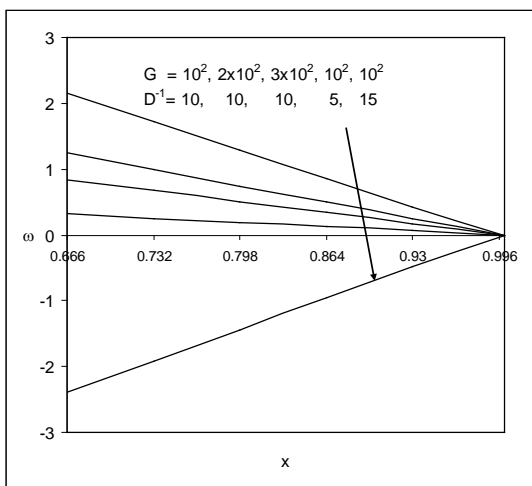


Fig. 35 : Variation of ω with G, D^{-1} at $y = \frac{2h}{3}$ level

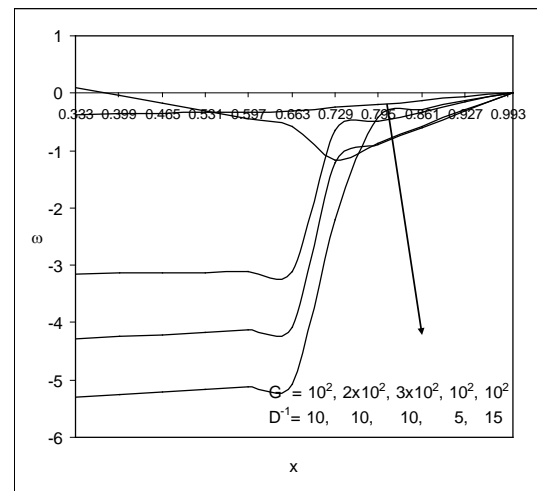


Fig. 36 : Variation of ω with G, D^{-1} at $y = \frac{h}{3}$ level

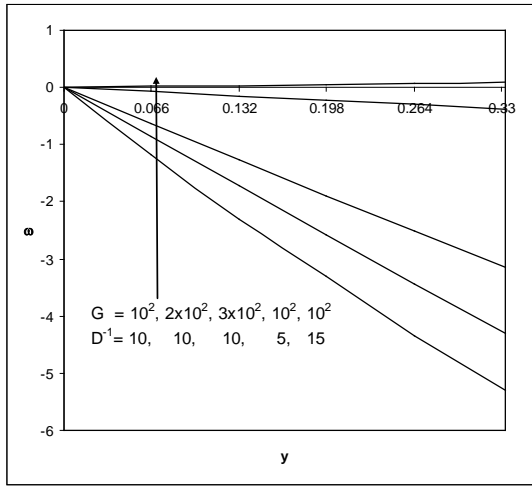


Fig. 37 : Variation of ω with G, D^{-1} at $x = \frac{1}{3}$ level

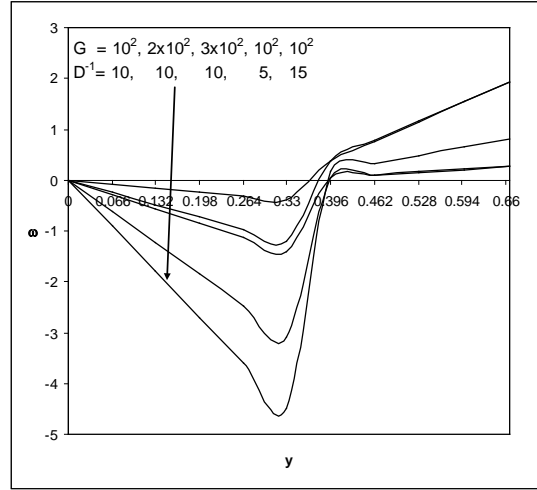


Fig. 38 : Variation of ω with G, D^{-1} at $x = \frac{2}{3}$ level

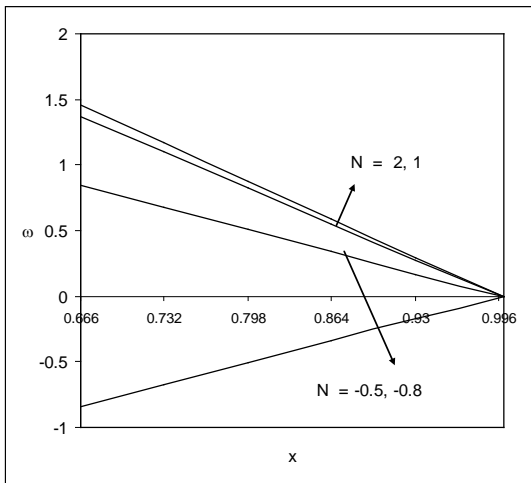


Fig. 39 : Variation of ω with N at $y = \frac{2h}{3}$ level

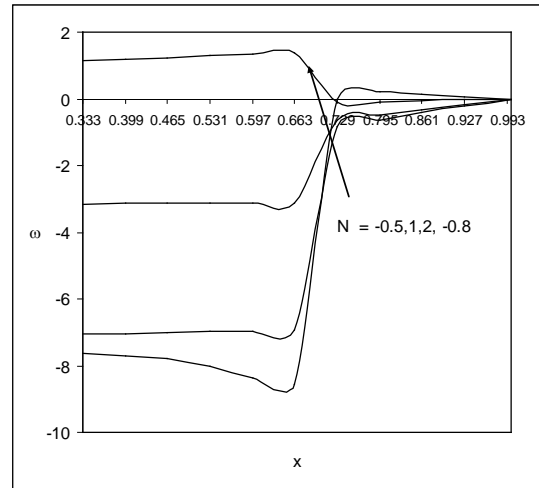


Fig. 40 : Variation of ω with N at $y = \frac{h}{3}$ level

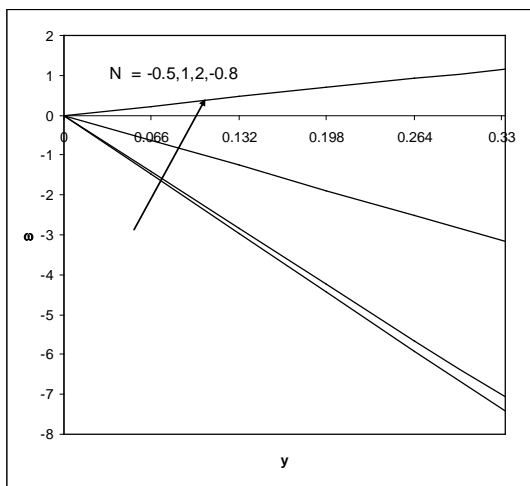


Fig. 41 : Variation of ω with N at $x = \frac{1}{3}$ level

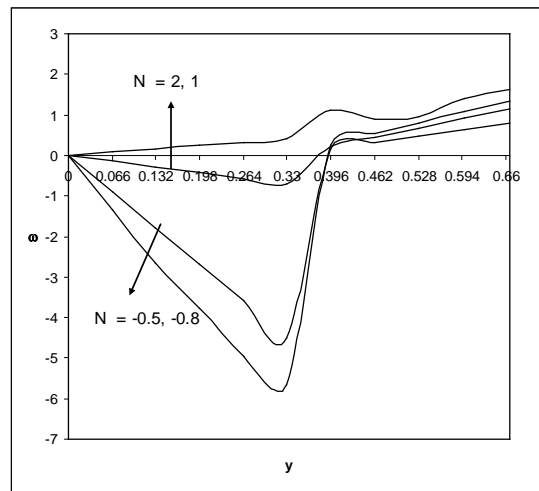


Fig. 42 : Variation of ω with N at $x = \frac{2}{3}$ level

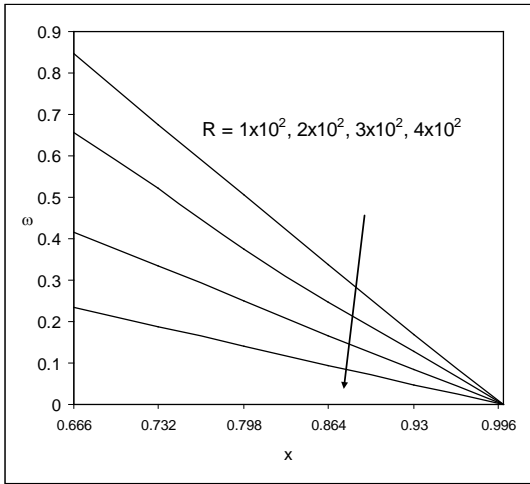


Fig. 43 : Variation of ω with R at $y = \frac{2h}{3}$ level

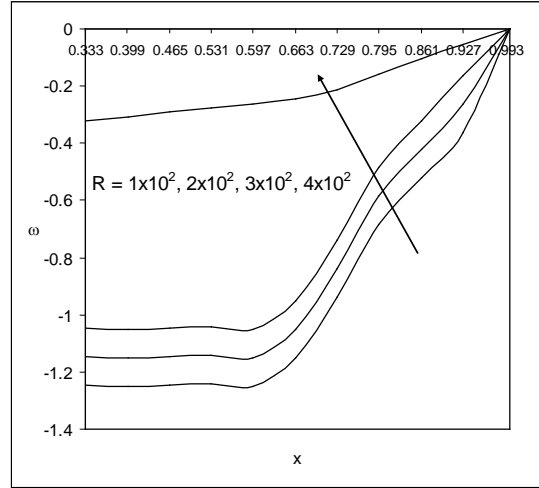


Fig. 44 : Variation of ω with R at $y = \frac{h}{3}$ level

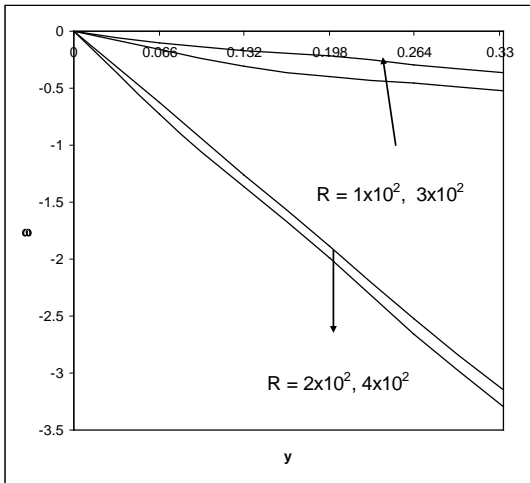


Fig. 45 : Variation of ω with R at $x = \frac{1}{3}$ level

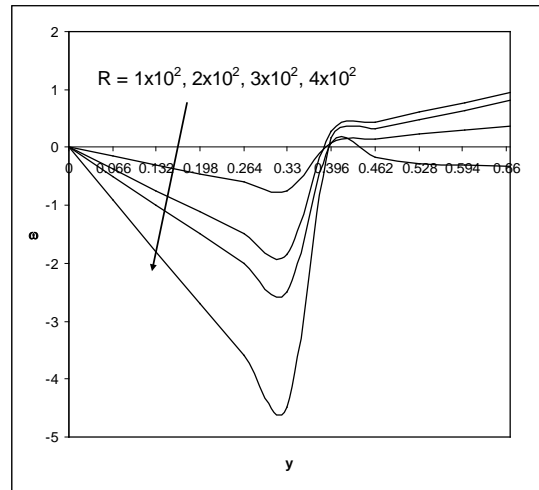


Fig. 46 : Variation of ω with R at $x = \frac{2}{3}$ level

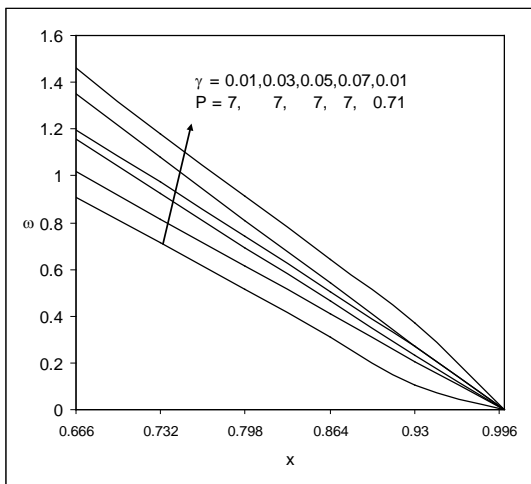


Fig. 47 : Variation of ω with γ, P at $y = \frac{2h}{3}$ level

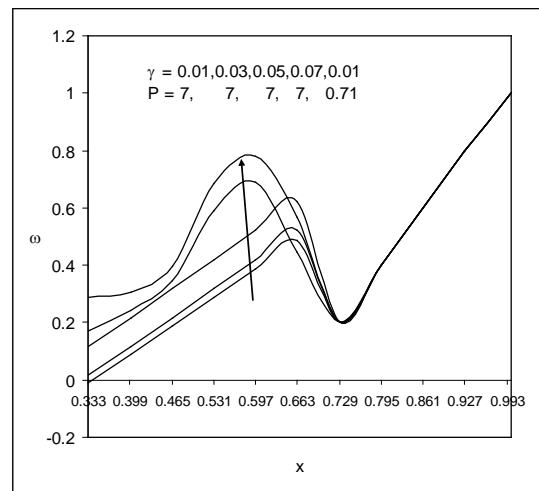


Fig. 48 : Variation of ω with γ, P at $y = \frac{h}{3}$ level

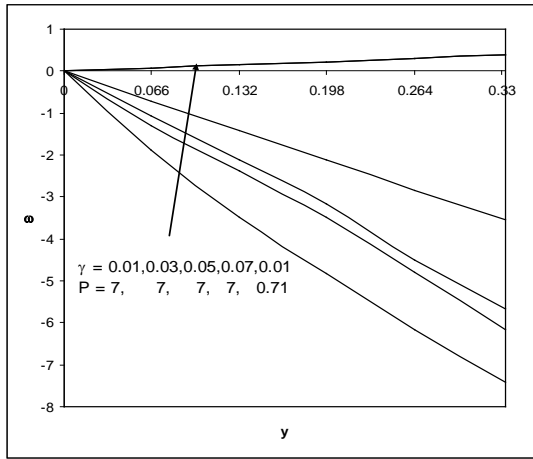


Fig. 49 : Variation of ω with γ , P at $x = \frac{1}{3}$ level

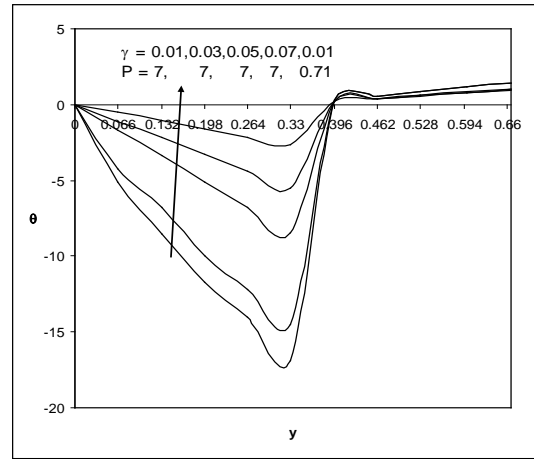


Fig. 50: Variation of ω with γ , P at $x = \frac{2}{3}$ level

The rate of heat transfer (Nusselt number) at $x=1$ shown in table 1 and 2 for different parametric values. It is found that the Nusselt number in the lower quadrants enhances with increase in G an increase in $G \leq 10^2$ reduces $|Nu|$ in the middle quadrant and reduces on the upper quadrant while for higher $G \geq 5 \times 10^2$ we notice depreciation in $|Nu|$ on the middle quadrant and enhancement on the upper quadrants. An increase in $D^{-1} \leq 10$ enhances $|Nu|$ at all the quadrants while for higher $D^{-1} \geq 15$, $|Nu|$ enhances on the lower quadrant and reduces on the middle and upper quadrants. With respect to buoyancy ratio N we find that $|Nu|$ reduces on lower and middle quadrants on enhances or upper quadrant with increase in $N > 0$ while an increase in $|N| < 0$ we notice a depreciation in $|Nu|$ at all the quadrants. With respect to micro polar parameter R ., we find that $|Nu|$ enhances with R on the lower and upper quadrants while on the middle quadrant, it reduces with $R \leq 0.1$ and enhances with higher $R \geq 0.3$. With respect to Prandtl number (P) we find that $|Nu|$ enhances on lower and upper quadrants and reduces on middle quadrant with increase in P . The variation of $|Nu|$ with density ratio (γ) shows that an increase in $\gamma \leq 0.03$, $|Nu|$ reduces on the lower and middle quadrants and enhances the upper quadrant while for higher $\gamma \geq 0.05$, we notice a reversed effect.

The rate of mass transfer (Sherwood number) on $x=1$ represented in tables 3 and 4 for different parametric variations. It is found that the Sherwood number enhances on lower and middle on a quadrant with increase in G while Sherwood number on the upper quadrant reduces with $G \leq 3 \times 10^2$ and enhances with higher $G \geq 5 \times 10^2$. The variation of Sh with D^{-1} shows that lesser the permeability of porous medium smaller the Sherwood number on all the three quadrants and for further lowering of permeability larger the Sherwood number. Sh with respect to buoyancy ratio. We find that when the molecular buoyancy force dominates over the thermal buoyancy force the rate of mass transfer enhances on the lower and upper quadrants and reduces in the middle quadrant when the molecular buoyancy forces are in the same direction and for the forces acting in opposite direction the Sherwood number depreciates on all three quadrants. An increase in $R \leq 100$ enhances the Sherwood number on the lower and middle quadrants and reduces on the middle quadrant and for higher $R \geq 0.3$ the Sherwood number reduces on the lower middle quadrant. The variation of ‘ Sh ’ with Prandtl number P Shows that lesser the thermal conductivity larger Sh on lower and upper quadrants and smaller on the middle quadrant. The variation of Sh with density ratio (γ) shows that an increase in $\gamma \leq 0.03$ reduces the Sh on all three quadrants and for higher $\gamma \geq 0.05$ we notice an enhancement in ‘ Sh ’ on the lower and upper quadrants and reduces on the middle quadrant (Table 4).

The couple stress (Cw) is shown in tables (5&6) for different parametric variations. It is found that an increase in G reduces the couple stress on the middle quadrant and enhances on the upper quadrant. Lesser the permeability of porous medium, Smaller the couple stress on the middle and the upper quadrants when the molecular buoyancy force dominates over the thermal buoyancy force the couple stress enhances when the buoyancy forces are same direction and forces acting in opposite direction Cw reduces on the lower quadrant. With respect to R we find that the Cw on the middle upper quadrant reduces with $R \leq 100$ and enhances with higher $R > 300$ (Table 5). An increase in the Prandtl number P reduces Cw on the all quadrants. With respect to density ratio γ , we find that the couple stress enhances with increase in γ . Thus the nonlinear density temperature relation results an enhancement in Cw on the quadrants (Table 6).

Table-1: Nusselt Number (Nu)

y	I	II	III	IV	V	VI	VII	VIII	IX	X
Nu1	2.08144	2.11484	2.1744	2.4852	2.244	2.0812	10.4804	2.5548	2.2628	1.97892
Nu2	-1.43732	-1.70824	1.65664	1.438	-0.14836	-0.39732	0.10692	-0.0216	-0.19124	-0.04432
Nu3	2.0156	2.0078	2.0436	2.2568	-0.0068	2.044	2.0912	1.98736	2.0764	1.99364
G	1×10^2	3×10^2	5×10^2	1×10^2						
D^{-1}	10	10	10	5	15	10	10	10	10	10
N	1	1	1	1	1	2	-0.5	-0.8	1	1
R	100	100	100	100	100	100	100	100	200	300

Table-2: Nusselt Number (Nu)

Y	I	II	III	IV	V
Nu1	2.08144	2.0044	2.1272	2.1376	2.7744
Nu2	-1.43732	0.071	-0.264	-0.04824	0.18768
Nu3	2.0156	2.1184	2.0644	2.064	2.2644
γ	0.01	0.03	0.05	0.07	0.01
P	7	7	7	7	1.71

Table-3: Shear wood number (Sh)

Y	I	II	III	IV	V	VI	VII	VIII	IX	X
Sh1	2.32784	2.5398	2.7564	3.1732	2.9756	2.3672	3.1868	2.19328	2.96	1.88492
Sh2	-0.46152	-0.93376	1.18156	-1.7148	-0.682	0.00572	-0.82036	0.1128	0.02288	-0.03676
Sh3	2.22972	2.09136	2.2052	2.4144	12.0256	2.2972	2.3448	1.9272	2.462	1.96684
G	1×10^2	3×10^2	5×10^2	1×10^2						
D^{-1}	10	10	10	5	15	10	10	10	10	10
N	1	1	1	1	1	2	-0.5	-0.8	1	1
R	100	100	100	100	100	100	100	100	200	300

Table-4: Shear wood number (Sh)

Y	I	II	III	IV
Sh1	2.32784	2.1656	2.5168	2.9028
Sh2	-0.46152	-1.0812	-1.06352	-0.02908
Sh3	2.22972	2.1828	2.4356	2.31332
γ	0.01	0.03	0.05	0.01
P	7	7	7	1.71

Table-5: Couple Stress ($C\omega$)

Y	I	II	III	IV	V	VI	VII	VIII	IX	X
$C\omega 1$	2	2	2	2	2	2	2	2	2	2
$C\omega 2$	19.9858	6.85	3.5364	7.632	14.328	48.088	4.8588	2.40768	5.0088	12.97388
$C\omega 3$	-1.21936	-5.24888	-5.6778	0.952	0.9252	-3.34612	-2.54032	-1.728	0.5084	22.05612
G	1×10^2	3×10^2	5×10^2	1×10^2						
D^{-1}	10	10	10	5	15	10	10	10	10	10
N	1	1	1	1	1	2	-0.5	-0.8	1	1
R	100	100	100	100	100	100	100	100	200	300

Table-6: Couple Stress ($C\omega$)

Y	I	II	III	IV	V
$C\omega 1$	2	2	2	2	2
$C\omega 2$	19.9858	44.0268	35.8264	118.436	12.6364
$C\omega 3$	-1.21936	-1.71156	-2.17528	-3.79176	-2.04512
γ	0.01	0.03	0.05	0.07	0.01
P	7	7	7	7	1.71

5. CONCLUSIONS

- ❖ The aim of this analysis is to investigate the effect of non linear density temperature variation on flow characteristics. The non linear coupled equations governing the flow heat and mass transfer have been solved by using Finite Element Method with linear approximations functions. The temperature, concentration, micro rotation, couple stress. Rate of heat and mass transfer have been discussed for different values of governing parameters.
- ❖ The important conclusion of these analysis are it is observed from the profiles that the actual temperature reduces with increases in $\gamma \leq 0.03$ and enhances with higher $\gamma = 0.05$. At $y=2h/3, h/3, x= 1/3$ levels. At $x=2/3$ level it reduces with increase in γ .
- ❖ The actual concentration enhances with $\gamma \leq 0.03$ and reduces with higher $\gamma \geq 0.05$ and again enhances with still higher $\gamma = 0.07$. At $y=h/3$ and $2h/3$ at both the vertical levels.
- ❖ The actual concentration enhances with γ the micro rotation (ω) reduces with $\gamma \leq 0.05$ and enhances with $\gamma \geq 0.07$. At $y=2h/3$ level. At $y= h/3$ and $x=1/3$ levels the micro rotation enhances with $\gamma \leq 0.03$ and reduces with higher $\gamma = 0.05$. At $x=2/3$ level the micro rotation enhances with γ .
- ❖ The rate of heat transfer reduces with $\gamma \leq 0.03$ and enhances with higher $\gamma = 0.05$ for the lower and middle quadrants while on the upper quadrants $|Nu|$ enhances with γ .

- ❖ The couple stress enhance with γ in all the three quadrants. The rate of mass transfer reduces with $\gamma = 0.03$ and enhances with higher $\gamma = 0.05$ and lower and upper quadrant while on the middle quadrant |Sh| reduces with γ .

6. REFERENCES

1. Al-Nimr, M.A: Analytical solution for transient laminar fully developed free convection in vertical annular., Int.J.Heat and mass transfer, Vol.36, pp.2385-2395(1993).
2. Badruddin, I.A., Zainal,Z.A., Aswatha narayana, seetharamu,K.N: Heat transfer in porous cavity under the influence of radiation and viscous dissipation, Int.comm.In Heat and MassTransfer 33,pp,491-499(2006).
3. Catton I: Natural convection in enclosure, Proc. 6th Int. Heat Transfer conf. Toronto, Canada. Vol. 6. Pp.13-31 (1978).
4. Catton I: The effect of insulating vertical walls on the onset of motion of fluid heated from below Int. J. Heat Mass Transfer 15, 665 (1972).
5. Chamka, A.J: Unsteady MHD Convective Heat and Mass transfer past a semi- infinite vertical permeable moving plate with heat absorption .Int.J.Eng.Sci.42, pp.217-230 (2004).
6. Chamka, A.J., Mallikarjuna, B., Bhuvana Vijaya,R and Prasada Rao, D.R.V: Heat and mass transfer in a porous medium filled rectangular duct with sores and Dufour effects under inclined magnetic field, Int. J. of Numerical Methods for Heat and Fluid Flow,Vol.24,No.7, pp.1405-1436 (2014).
7. Cha O-Kaung Chen and Tsan – Huihsu: Natural convection of micropolar fluids in a Rectangular Enclosure: Int. J. Eng. Sci. Vol. 34. 4. pp. 407-415 (1966).
8. Davis S.H: J. Fluid Mech. 30. 465 (1967).
9. Eringen, A.C: Int. J. Eng. Sci., 2, 205 (1964).
10. Eringen, A.C: J. Math Mech. 16, 1 (1977).
11. Eringen, A.C.: J. Math Anal. Appl. 38, 480 (1972).
12. Gnanaprasunamba. K and Sulochana. C: Convective heat and mass transfer flow of a Rectangular Duct With sores and dufour effects and heat sources. Int. J. of engineering research and applications, volume 4, pp.157-192 (2014).
13. Haajizadeh, M. and Tien, C.L: Trans ASME, J. Heat Transfer 105, 803 (1978).
14. Jena, S.K and Bhattacharya, S.P: Int. J. Eng. Sci., 24, 69 (1986).
15. Kamotani., Wang, L.W., Ostrach, S. and Jiang,H.D: Experimental study of natural convection in shallow enclosures with horizontal temperature and concentration gradients, Int. J. Heat Mass transfer, Vol.28, PP.165-173 (1985).
16. Krishna, D.V: non-darcian convection flow in a circular duct partially filled with porous medium Journal of Engineering Physics and Thermophysics, Vol. 82, No. 5 (2009).
17. Ostrach S: Adv. Heat Transfer, 8, 161 (1972).
18. Ozoe H., Yamamoto K., Sayama H. and Churchill S.W.: Int. J. Heat Mass Transfer 17, 1209 (1972).
19. Ozoe H. and Sayama H.: Int. J. Heat Mass Transfer, p. 18, 1425 (1975).
20. Rajakumari, P: Convective Heat and Mass Transfer flow Micro polar fluid in a Rectangular duct with heat sources, Int. J, Engg Technology, Volume 5, p. 3 (2016).
21. Samuels, M.R. and Churchill S.W: Alche, J. 10, p.110 (1967).
22. Sesha Sailaja, M and Sarojamma, G: Effect of non-linear density temperature variation on convective heat transfer of a viscous fluid through a rectangular cavity, International Journal of Mathematical Archive, Vol. 4(2), pp.78-89 (2013).
23. Shanthi, G., Jafarunnisa, S. and Prasada Rao, D.R.V: Finite element analysis of convective heat and mass transfer flow of a viscous electrically conducting fluid through a porous medium in a rectangular cavity with dissipation, International journal of Electrical, Electronics and computing Technology(IJEECT), Vol 2, No.4, pp. 29-34 (2011).
24. Umadevi, B and Bhuvana Vijaya, R: Finite Element Analysis of double-diffusive heat transfer flow in rectangular duct with thermo-diffusion and radiation effects under inclined magnetic field, IJMA-7(4), pp. 71-98 (2016).
25. Veera Suneela Rani, A., Sugunamma,V and Sandeep, N: Radiation Effects on Convective Heat and Mass Transfer Flow in a Rectangular Cavity, International Journal of Innovation and Applied Studies ISSN 2028-9324 Vol 1(1), pp. 118-152 (2012).
26. Verschoor, J.D and Greebler, P: Heat Transfer by gas conduction and radiation in fibrous insulation trans.Am.Soc.Mech.Engrs., pp. 961-968 (1952).
27. Walker K.L. and Homsy G.M.: J. Fluid Mech. 87, P. 449 (1978).
28. Wang M., Tsuji T. and Nagana: Mixed convection with flow reversal in the thermal entrance region of horizontal and vertical pipes. Int. J. Heat Mass Transfer, 37, pp. 2305-2319 (1994).
29. Wang M. and Tsan – Huihsu: Int. J. Heat and Mass Transfer, 43, pp. 1563-1572 (2001).
30. Wilson G.L. and Rydin R.A.: Int. J. Numer. Mech. Fluids 10, p. 35 (1990).

Source of support: Nil, Conflict of interest: None Declared.